UNIVERSIDADE D
COIMBRA

Inês Filipa Fornelos do Carmo

FLUID STRUCTURE INTERACTION ON ENGINE BLADES MANUFACTURING

Study and Improvement of the Experimental Setup

VOLUME 1

Dissertação no âmbito do Mestrado Integrado em Engenharia Mecânica, Área de Especialização de Energia e Ambiente, coorientada pelo Professor José Manuel Baranda Moreira da Silva Ribeiro e pelo Professor Michel Arrigoni apresentada ao Departamento de Engenharia Mecânica, da Faculdade de Ciências e Tecnologia da Universidade de Coimbra.

Julho de 2022

1 2 9 0

FACULDADE DE CIÊNCIAS E TECNOLOGIA UNIVERSIDADE D COIMBRA

Fluid-Structure Interaction on Engine Blades Manufacturing

Submitted in Partial Fulfilment of the Requirements for the Degree of Master in Mechanical Engineering in the speciality of Energy and Environment

Interação Fluido-Estrutura na Manufatura de Pás de Turbina

Author

Inês Filipa Fornelos do Carmo

Advisor[s]

Prof. Michel Arrigoni

Prof. José Manuel Baranda Moreira da Silva Ribeiro

Jury

President	Professor Doutor **Almerindo Domingues Ferreira**
Vowel[s]	Mestre **Pedro Miguel Martins de Brito**
Advisor	Professor Doutor **José Manuel Baranda Moreira da Silva Ribeiro**

Institutional Collaboration

1 2 9 0 FACULDADE DE CIÊNCIAS E TECNOLOGIA UNIVERSIDADE D COIMBRA

Universidade de Coimbra

ENSTA Bretagne

École Nationale Supérieure de Techniques Avancées Bretagne

Coimbra, July, 2022

ACKNOWLEDGEMENTS

The presented work would not be possible without the support of several people that I would like to present my thanks and acknowledgements:

To Professor José Baranda for motivating me and providing me with the opportunity of participating in this internship.

To Professor Michel Arrigoni and Steven Kerampran for the patience, availability and knowledge that they passed to me.

To Researcher Julien Le Clanche and Professor Martin Monloubou for their availability and kindness during my time in ENSTA Bretagne.

To my family and Renato for the unconditional support during this work and my journey in university.

Abstract

The present dissertation had as objective the study and improvement of the experimental setup for the fluid-structure interaction on engine blades manufacturing for the achievement of higher velocities and a steady free surface, during a curricular internship in ENSTA Bretagne. The process in question aims to reduce the rejected parts of engine blades in the casting process that would allow to achieve lighter hollow metallic parts that include a cooling system for enhancing mechanical performances.

All the stages of the internship are addressed, beginning with an overview of the evolution of the main parts of the project so far. Several experiments and results are mentioned on which the improvements proposed were based.

Experiments were performed, during this internship, to evaluate the impact of the pressure setup in the fluid behaviour. These experiments allowed to find certain difficulties that were causing constrains in the results.

Simulations were performed to study some pieces of the setup in detail. A structural analysis and a study of the fluid dynamic were conducted to analyse the structural integrity of the redesigned pieces, as well as, to evaluate the interaction of the fluid with specific parts of the setup.

A new experimental setup was proposed to minimize the challenges encountered and improve the results. Several pieces were redesigned, bearing in mind the objective of having a free surface as stable as possible and that speeds in the order of m/s are achievable.

Keywords: Fluid-structure interaction, Experimental setup, Turbulence, Cast manufacturing, Fan blade

Resumo

A presente dissertação tem como objetivo o estudo e melhoria da instalação experimental para a interação fluido-estrutura na manufatura de pás de turbina, de modo a atingir velocidades elevadas e uma superfície livre constante, durante o decorrer de um estágio curricular na ENSTA Bretagne. O processo em questão tem como objetivo a redução do número de pás de turbina com defeito durante o processo de manufatura, que permite a criação de peças metálicas ocas e mais leves com um sistema de arrefecimento para melhorar a performance mecânica.

Todas as etapas do estágio são mencionadas, começando por um resumo da evolução das partes principais do projeto até á data. Experiências, resultados e melhorias implementadas são referidas para a contextualização e melhor compreensão do projeto.

Foram realizadas experiências para avaliar o impacto da instalação de pressão no comportamento do fluido. Estas experiências permitiram encontrar certas dificuldades que causavam constrangimentos nos resultados obtidos.

Foram realizadas simulações para o estudo de algumas peças em detalhe. Análise estrutural e o estudo da dinâmica do fluido foram realizados para analisar a integridade estrutural das peças redesenhadas, como, para avaliar a interação do fluído com partes específicas da instalação.

Uma nova instalação experimental foi proposta, de maneira a minimizar os desafios encontrados e melhorar os resultados. Várias peças foram redesenhadas, tendo em mente o objetivo de se ter uma superfície livre estável e velocidades na ordem dos m/s serem alcançadas.

Palavras-chave: Interação fluído-estrutura, Instalação experimental, Turbulência, Fundição, Pás de turbina

Contents

LIST OF FIGURES

LIST OF SYMBOLS AND ACRONYMS/ ABBREVIATIONS

List of Symbols

A [m^2]– Internal area of the setup

f [Hz] – Acquisition frequency

g – Gravitational acceleration

L [m] – Height of the water column

L_c [m]– Core length

M [m]– Diameter of the cell size of the honeycomb

$\dot{P}_c$ [$Pa \cdot s^{-1}$] – Derivative of the pressure inside the tank

R – Reynolds number

S [m^2]– Area of the plexiglass vein

S_c – Water surface in the metal tank

V [m^3] – Volume in the tank

U_a [m/s] – Ascendent flow velocity

U_m [m/s] – Water minimum velocity

ρ [kg/m^3] – Water density

μ [$Pa \cdot s$] – Water dynamic viscosity

Acronyms/Abbreviations

PVC – Polychlorure de Vinyle

PVDF – Polyvinylidene fluoride

PIV – Particle Image Velocimetry

DAQ – Data Acquisition Device

VOF – Volume Fluid Model

1. INTRODUCTION

The manufacturing of engine blades is a process where a great number of blades are produced with defects due to fused metal-core interaction during casting, which invalidates their use. In an effort to improve the process of manufacturing, Safran a company with expertise in the field of Aeronautics through join efforts with ENSTA Bretagne is conducting a study to understand in which conditions the defects occur during the moulding process. The study of this process would allow reducing the manufacturing costs to design hollow metallic blades that provide better performances, since they are lighter and easier to cool down with mechanical performances allowing resisting impacts.

1.1. State of the Art

The moulding process is governed by fluid-structure interaction, during this process the structure (core) has a displacement where even breakage of this structure can occur (Palut, 2021) creating defects on the manufactured blades. A benchmark has been developed at ENSTA Bretagne to study the fluid-structure interaction. Preliminary experiments, Croci et al. 2019 and Palut, 2021, could give a good description of the fluid structure interaction at impact velocities lower than 0.8 m/s. However, they could point out that for velocities higher than 0.8 m/s, the rising liquid surface is turning to turbulent flows with sometimes bubbles. It was concluded that to obtain a better description of the fluid-structure interaction for higher velocities, modifications in the setup should be implemented.

1.2. Goals and Motivation

The present dissertation had origin in the high-performance requirements for the aviation industry and the environmental challenges that led Safran to launch a project to master the manufacture of a new technology for turbine blades.

The moulding process permits the appearance of deformations on the blades. Safran is working on the study of the origin of the defects using a numerical approach based on the forces that the fluid exercises on the components of the ceramic mould.

In partnership with ENSTA Bretagne an experimental setup was created to simulate the moulding process, to better understand the conditions in which the core offset occurs and the phenomena itself from the fluid point of view. Throughout the project several constraints were encountered which limited the results.

The main goal of this work is to study and improve the experimental setup for the achievement of better results that are in accordance with the numerical results.

1.3. Methodology adopted

The chapters presented cover the main phases of the work done to improve the future results delivered. In this document, six chapters can be found and are sorted in respective order of the conducted work:

- In first chapter is presented the subject of the performed work, the goals and importance for its execution and the adopted methodology;
- The second chapter is intended to present the progress of the project and the status of the experiments carried out so far. The experimental setup was introduced, the experimental campaign was explained, including, the measurement methods used and experiments done, finally, the improvements made to get better results were addressed.
- In third chapter the conducted experiments are addressed, where the influence of the pressure setup is evaluated in the behaviour of the flow and in the velocity achieved in the setup;
- In fourth chapter several new pieces for the setup were designed to improve the results obtained and to solve and minimize most of the problems and constrains found after the performed experiments.
- In fifth chapter two software's are introduced to conduct structural analysis and the study of the different parameters of the flow near the internal pieces of the setup.

- The last chapter presents the derived conclusions from the performed work during the internship as well as future prospects for the addressed project.

2. EXPERIMENTAL FRAMEWORK

2.1. Project Framework

The moulding process for production of the blades consist in casting superalloys in a ceramic mould (the shell) and insert a ceramic piece (the core) into the mould. This process originates a hollow metal piece with an internal cooling circuit path where a gas circulates during the operation of the blade at high temperatures. The wall thickness of the blade is less than one millimetre what makes the process of manufacturing delicate. After the casting a cooling process occurs in which local deformations appear duo to the range of temperatures and to the different properties of the materials used in this process. During the casting and cooling process, the core displacement occurs which results in parts that can´t be used. The core displacement can occur because of the impact between the fluid and the core during the moulding process or an extreme case in which the core displacement originated breakage.

Safran used the FLOW-3D® tool to model the fluids used in moulding and filling problems. To validate this methodology of production a comparison between the computational and experimental results needed to be carried out. The results obtain in the experimental setup were very similar to the results obtain by Safran for a range of velocities. However, in tests in which higher velocities (1 m/s) were practiced the experimental results had a high level of uncertainty.

2.2. Experimental Setup Design

2.2.1. Testbench

The experimental setup was based on the one proposed by Sanitas *et al.*, 2018. In the experimental setup water was used as a reference liquid because of its semi-similar viscosity with molten metal (Croci *et al.*, 2019). However, the Reynolds number is significantly different because of the density parameter of the two fluids. The Reynolds number for water is represented by Equation (2.1):

$$R_e = \frac{\rho U L_c}{\mu} = 1.5 \times 10^4 \tag{2.1}$$

Being that the minimum water velocity used in the tests is $U_m = 0.15\ m/s$,the core with the smallest length is $L_c = 0.1\ m$ long, ρ is the water density and μ the water dynamic viscosity (Palut, 2021). This value of number of Reynolds is considered to be in turbulent regime, just like the molten metal in the industrial process. In the Figure 2.1 the test bench is presented and is composed by the next elements:

- 1- A metallic water tank with approximately 30 litters, which has incorporated a temperature and pressure sensor.
- 2- An air tank connected to the air network is maintained to a constant pressure with the assistance of a pressure reducer.
- 3- A pressure regulator connected to the pressure sensor in the tank and to the air tank.
- 4- A plexiglass vein with a square section.
- 5- Honeycomb located at the bottom of the plexiglass vein (not visible in Figure 2.1).
- 6- A core (different ones were used) with simple geometric designs.
- 7- Different 3D printed pieces that allow the attachment of the parts referred.

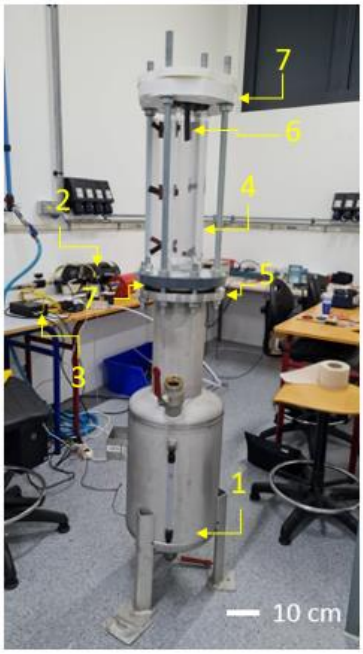

Figure 2.1. Test bench of the experiment at ENSTA Bretagne.

The experimental setup is composed of two attachment pieces, one at the top of the metal tank and the other at the top of vein. The first attachment piece keeps together the vein

and the honeycomb and allow the water to pass from the tank to the vein. The second attachment piece incorporates de vein and the core, whereby the core is attached to this piece with a screw. Four beams and several nuts compressed these numerous parts together.

2.2.2. Testing veins and cores

Different veins with different interior dimensions were produced with 600 mm x 600 mm, 800mm x 20mm and 800 mm x 800mm each one has 100mm x 100mm of exterior dimension.

Different cores (Figure 2.2, Figure 2.3) were considered for the experiments:

- Two axisymmetric with ends: flat and hemispherical
- Symmetric oval core
- Asymmetric NACA 9320 wing profile
- Symmetric oval core with inclination
- Cores provide by Safran

The symmetrical oval core, NACA 9320 and a symmetrical oval core with inclination were produced in Agilus resin, a material compatible with 3D printing. The symmetrical oval core with inclination is very similar to the symmetrical oval core, but with a 45º degree inclination at the tip of the core. The two axisymmetric cores were produced in a rigid polymeric material (PVC). The cores provide by Safran are from ceramic.

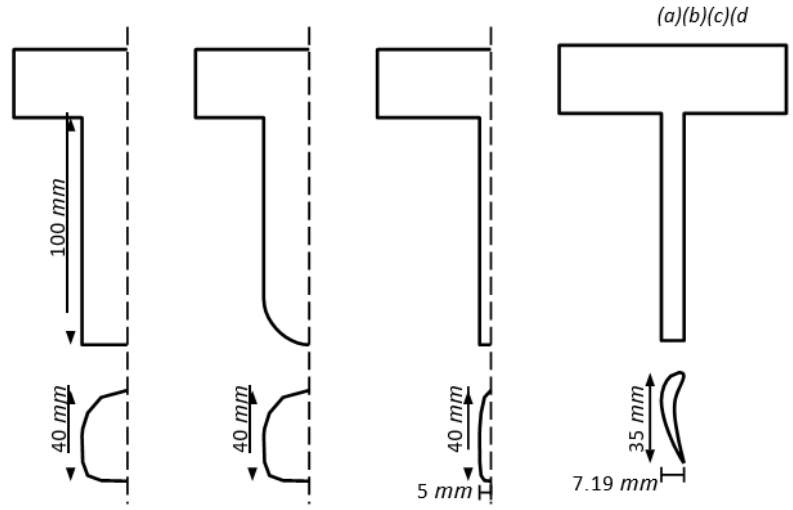

Figure 2.2. Cores with simplified geometric shapes: axisymmetric (a) flat and (b) hemispherical, symmetric (c) oval and asymmetric (d) NACA 9320 wing profile (Croci *et al.*, 2019).

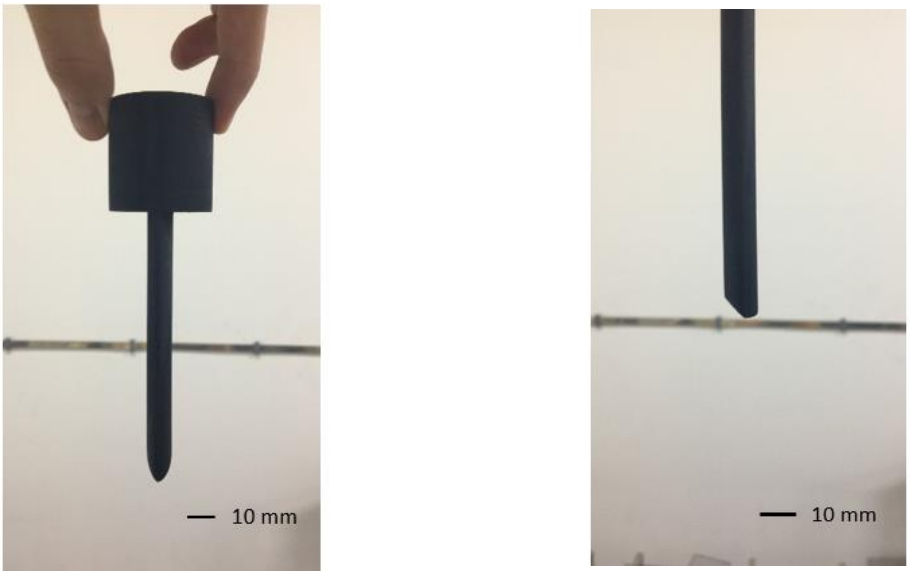

(a) (b)

Figure 2.3. (a) Symmetrical oval core with inclination.; (b) Tip detail of the Symmetrical oval core with inclination.

2.3. Experimental campaign

2.3.1. Measurement methods

Different methods for the displacement measurement were considered and implemented.

To visualize the phenomena and measure the core displacement a high-speed camera was implement (Figure 2.4). The high-speed camera has an acquisition frequency of 100 < f < 1000 Hz (normally f =500 Hz). A source of light is needed in front of the camera otherwise the camera can't visualize the impact of the water in the core.

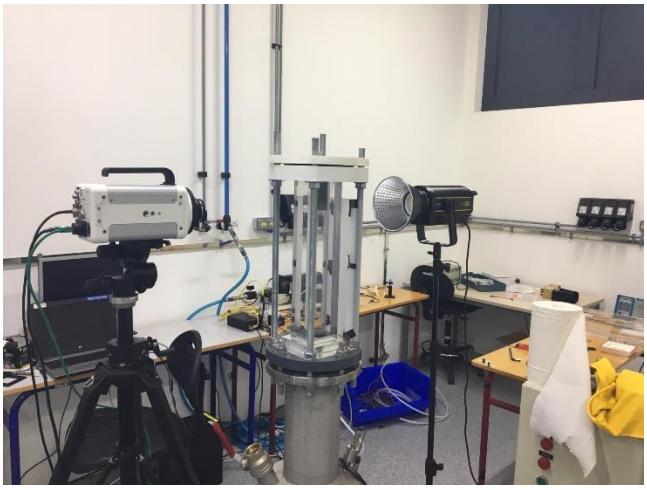

Figure 2.4. Experiment setup with the high-speed camera and light.

A PVDF sensor (Figure 2.5) was considered, to be implemented at the flat end of the cores to measure the dynamic impact pressure with the water. However, this implementation would be very intrusive and from difficult achievement.

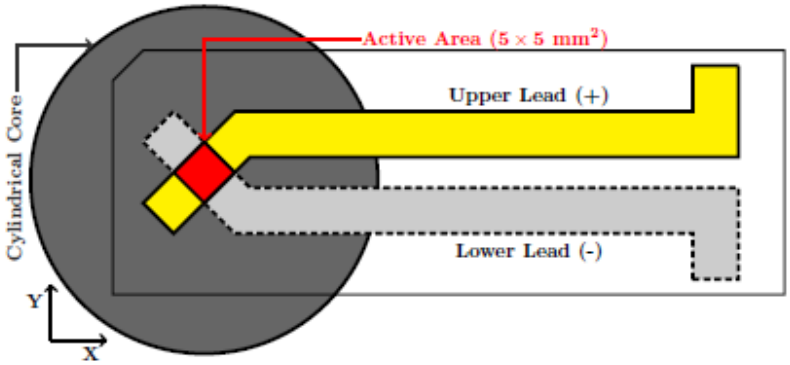

Figure 2.5. Proposal of implementation of a PDVF sensos in a cylindrical core (Croci et al., 2020).

A particle image velocimetry (PIV) was implemented (Figure 2.6) as an optical method to measure the velocity profile of the flow and to observe the water surface before and after impact. The water was seeded with polyamide particles of average size of 100 μm. The 5 W diode laser had wavelength of 532 mm. The images acquisition of the impact between the water and the core is done by the camera at 500 images.s^{-1} with a resolution of 800x600 $pixels^2$ (Croci *et al.*, 2020).

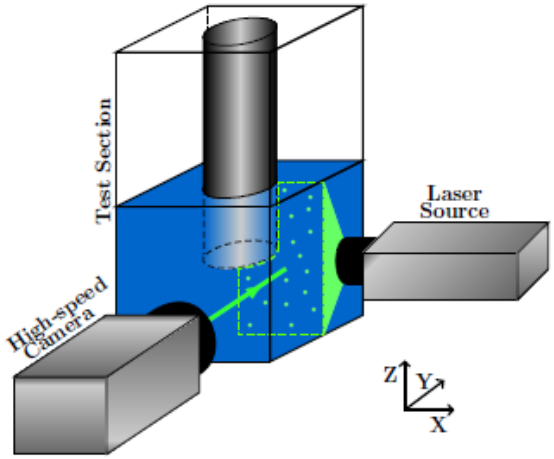

Figure 2.6. Scheme of the PIV setup (Croci *et al*., 2020).

Schlieren Visualization is a visualization method (Figure 2.7) where light rays are bent whenever they encounter changes in density of a fluid (‘Schlieren Flow Visualization’ n.d.). A light source is positioned near of the plexiglass vein in a way that the light beams reflected from the mirror form parallel rays that pass throughout the test section. On the other side of the setup another mirror reflects the light beams into a high-speed camera. A knife is used at the focal point of the beam to cut the light beam in two, blocking one part of the beam from reaching the camera. This way, only the light rays that are deflected (red beam) reach the camera with full intensity creating a light gradient in the acquired image.

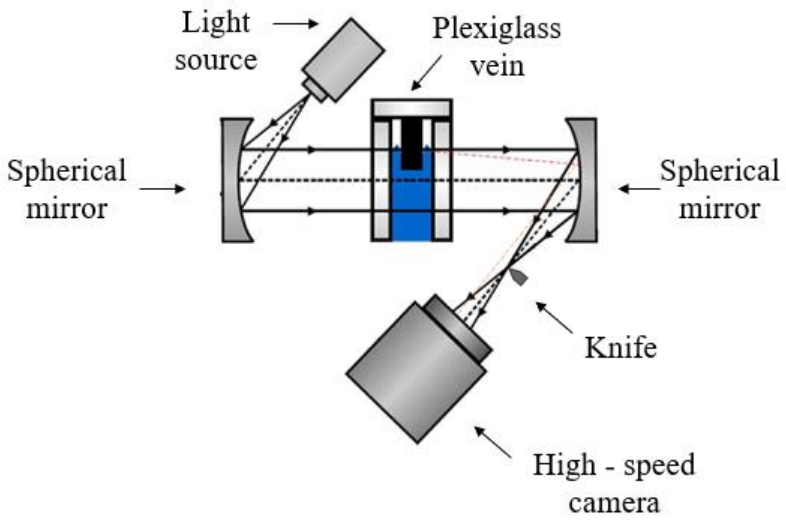

Figure 2.7. Setup schematic for Schlieren Visualization (Palut, 2021).

2.3.2. Experiments

Several observations and experimental results were obtain using the three veins and the different cores referred using the high-speed camera, PIV and Schlieren visualization.

In order to determine the ascendant flow velocity of water two methods were used (Figure 2.8):

- The equation **(2.2)**, Liu *et al.*, 2015, that uses the pressure in the tank.

$$U_a = \frac{1}{g\rho(1+\frac{S}{S_c})} \times \dot{P}_t \tag{2.2}$$

Being that $\rho = 1000\ kg/m^3$ *c*orresponds to the density of water, g is the gravitational acceleration, $S = 0.064\ m^2$ is the internal area of the plexiglass vein, $S_c = 5.71 \times 10^{-2} m^2$ is the area of the water surface in the tank without the metal tube in the interior and $\dot{P}_t$ is the derivative of pressure inside the tank.

- Analysis of images recorded by the high-speed camera.

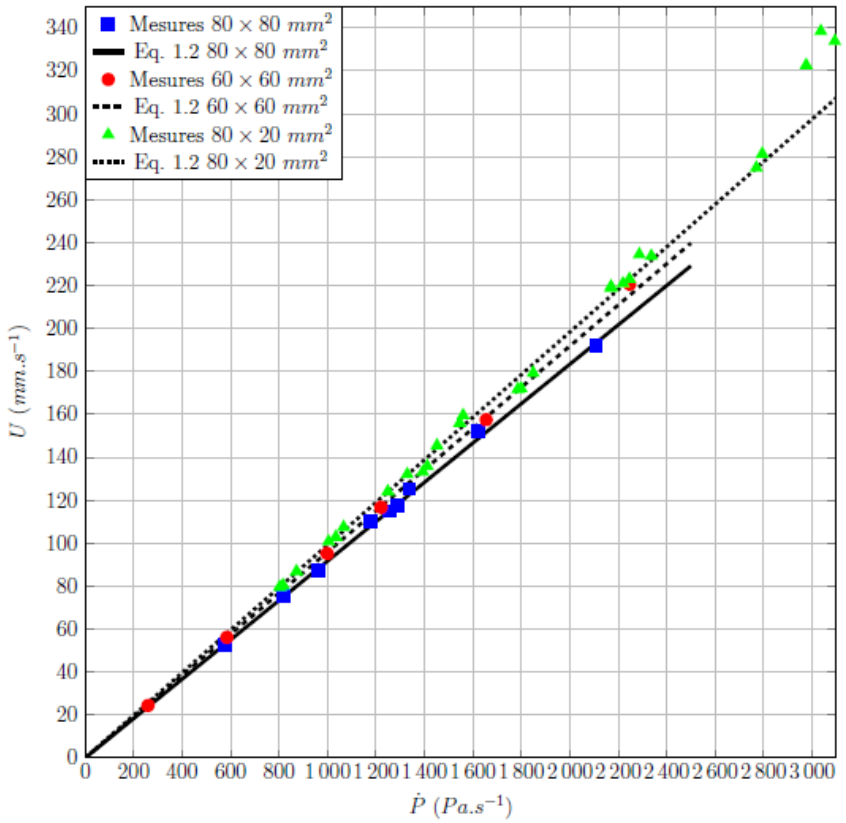

Figure 2.8. Velocity obtained by two methods in order of the pressure in the interior of the tank ($\dot{P}_t$), being that the Equation 1.2 mentioned in the Figure is the Equation 2.2 of this document. (Croci *et al.*, 2020).

To visualize and comprehend how the fluid behaves before reaching the core and during the intersection with it (Figure 2.9), the high-speed camera was used at low velocities (less than 1 m/s). Several experiments were done at several velocities and with different cores.

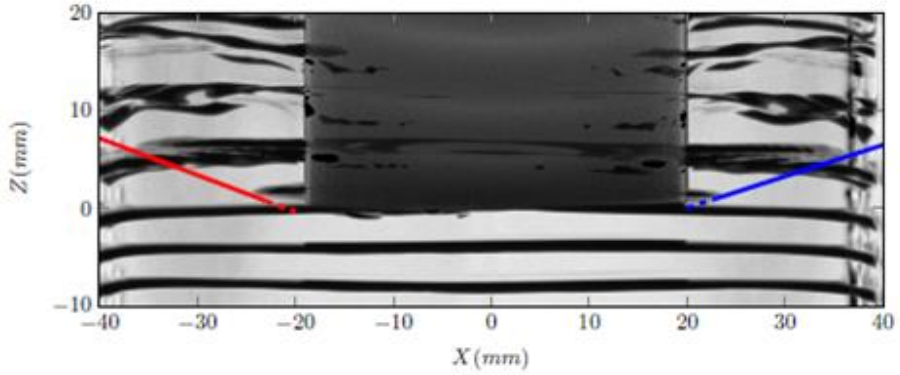

Figure 2.9. Superposition of images of the water surface reaching the core at $\dot{P} = 1137.8\ Pa.s^{-1}$ ($U = 104.3\ mm.s^{-1}$), where the red and blue lines represent the evolution of the wavefront on the left and right sides of the core (Croci *et al.*, 2020).

The interference of the walls of the vein in the velocity and the behaviour of the rising surface of the fluid was studied by PIV. In fact, the walls modify the surface of water as seen in Figure 2.10 .

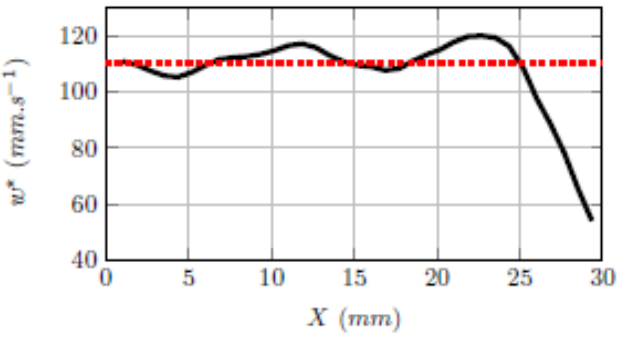

Figure 2.10. Vertical axis velocity (w^*) before impact, whereas the dotted red curve indicates the ascent speed $U = 110\ mm.s^{-1}$ (Croci *et al.*, 2020).

In order to measure the core offset and to understand the behaviour of the core during the impact with water, the hight speed camera was used to record in detail the end of the core (Figure 2.11).

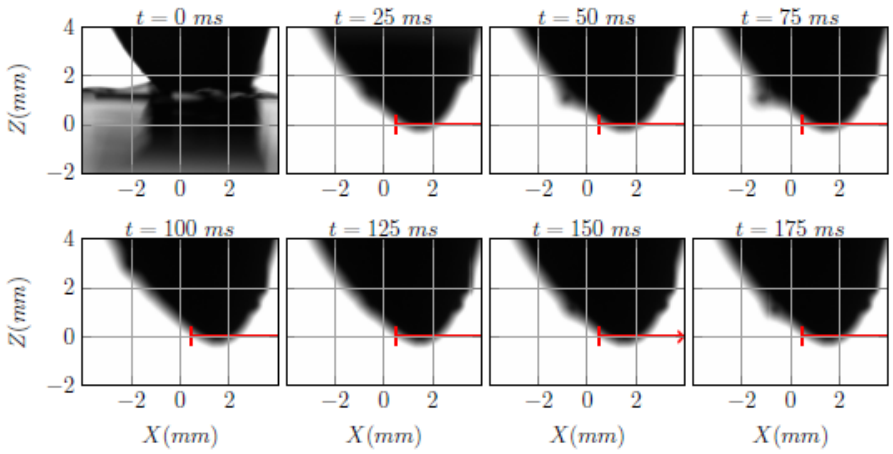

Figure 2.11. Impact of the water in the Symmetrical oval core with inclination at a speed of $U = 252\ mm.s^{-1}$ with $\Delta t = 25\ m.s$. The displacement is detected in the red line at Z = 0 mm (Croci *et a*l., 2020).

After several experiments done it was concluded that the measurement of the core displacement required a more efficient technique, it was proposed an increase of the zoom of the high-speed camera, a new technique like heterodyne velocimetry that could be implemented together with the hight speed camera or image analysis by improving the quality of visualization.

2.4. Improvements

2.4.1. Framework and work progress

With the setup installed the maximum velocity achieved is of 25 cm/s, since Safran goal is to reach a velocity of 1 m/s the only way to achieved this is take out the pressure regulator. However, without the pressure regulator the free surface of water rising turns into a jet (Figure 2.12) which is not reproducible and doesn´t correspond to the industrial process.

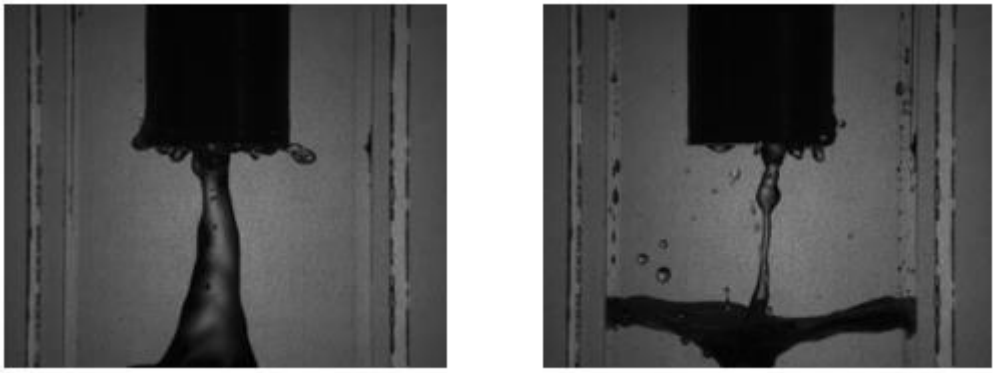

Figure 2.12. Free surface of water in contact with the axisymmetric flat core in two different tests at $U = 0.9\ m/s$ (Croci *et al.*, 2020).

A 3D printed honeycomb was proposed with the intention of breaking turbulences at the origin of the jet (Figure 2.13). This honeycomb is placed at the end of the vein, to promote a homogenous flow without having a severe pressure drop. A few samples were printed, the first one has 20 mm of height, hexagonal meshes of 9,75 mm inner diameter and 0,25 mm wall thickness, which represents a free surface of 93% (Palut, 2021).

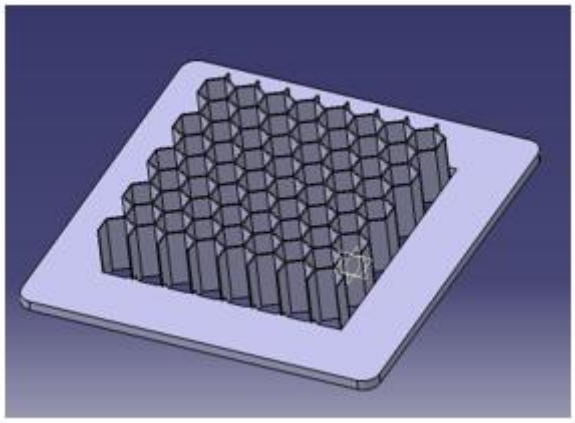

Figure 2.13. Representation of the first honeycomb implemented in 3D (Palut, 2021).

With the implementation of the honeycomb the behaviour of the free surface stabilized considerably (Figure 2.14), which allows the repeatability of the results, however, is possible to see the appearance of small turbulences and bubbles.

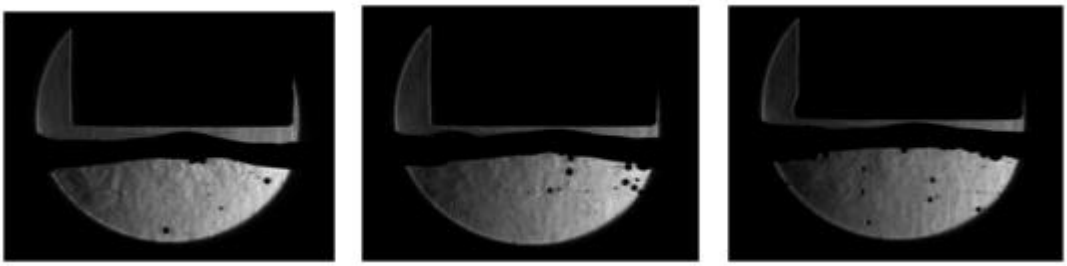

Figure 2.14. Observation of the free surface by Schlieren Visualization at $U = 0.77\ m/s$ with the first honeycomb produced for3 different tests (Palut, 2021).

Different designs of honeycombs (Figure 2.15) were printed and implemented with the goal of improving the first one. One honeycomb had the double of height and the other one had half of the mesh size.

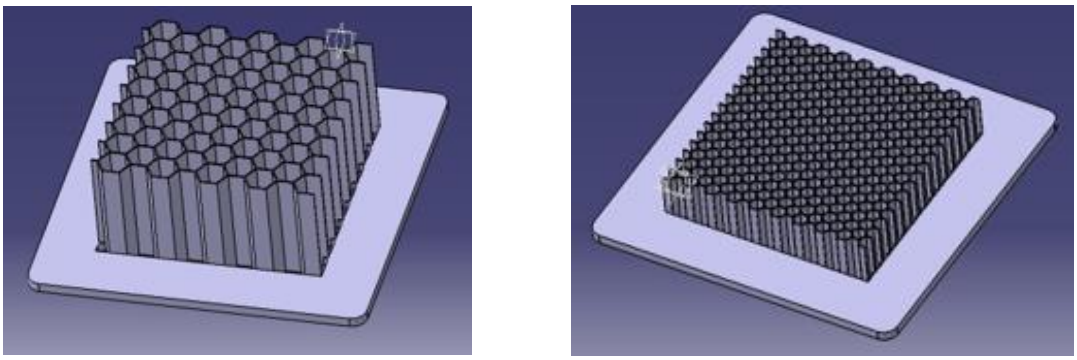

(a) (b)

Figure 2.15. (a) Honeycomb with double height; (b) Honeycomb with half of cell size.

Nevertheless, this other two options had a worse performance than the first one. In the Figure 2.16 is visible the state of the fluid with several bubbles and an unsteady surface.

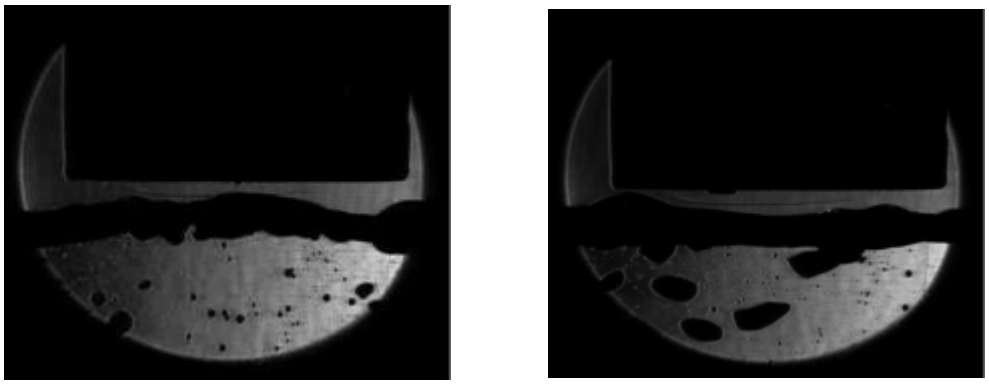

(a) (b)

Figure 2.16. (a) Honeycomb with double height; (b) Honeycomb with half of cell size.

2.4.2. Experiments

Several tests were done to characterize the water rising velocity with the upstream pressure. It is concluded that due to several limitations the ideal vein to use in the tests is the 800×800 mm. As mentioned, the velocity limitations caused by the pressure regulator didn´t allow to achieve higher velocities, since it´s range of use should be below 250000 Pa. For this reason, tests were conducted to velocities until 0.25 m/s (Figure 2.17), since with the pressure regulator the water surface is more stable, and the reproducibility and performance is better.

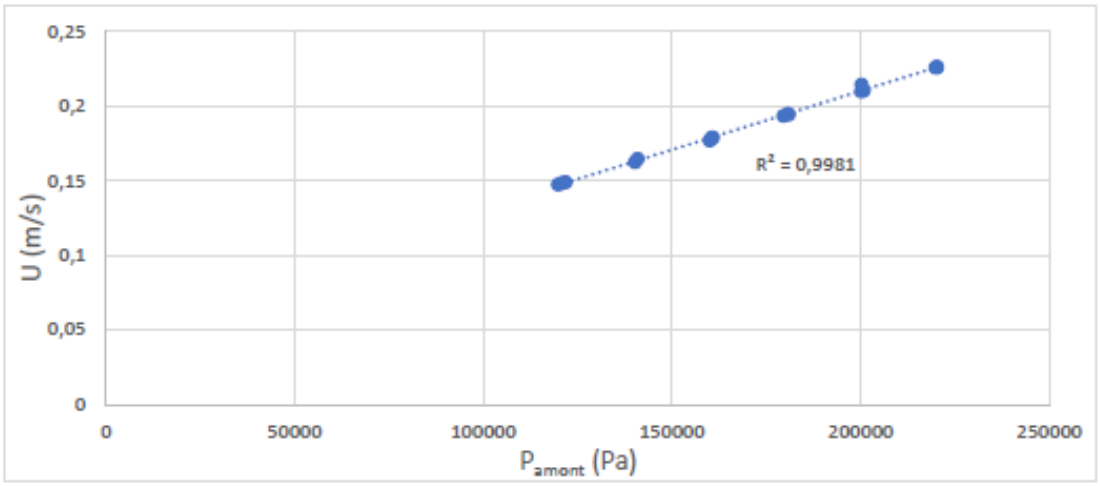

Figure 2.17. Relation between the water velocity and the upstream pressure with the pressure regulator implemented (Palut, 2021).

However, to achieve higher velocities was crucial to understand the relation between velocity and upstream pressure for pressure above 25 cm/s, which is only possible without the pressure regulator (Figure 2.18). It is clear, that without the pressure regulator higher velocities are achieved, but the free surface doesn´t have a stabilized behaviour.

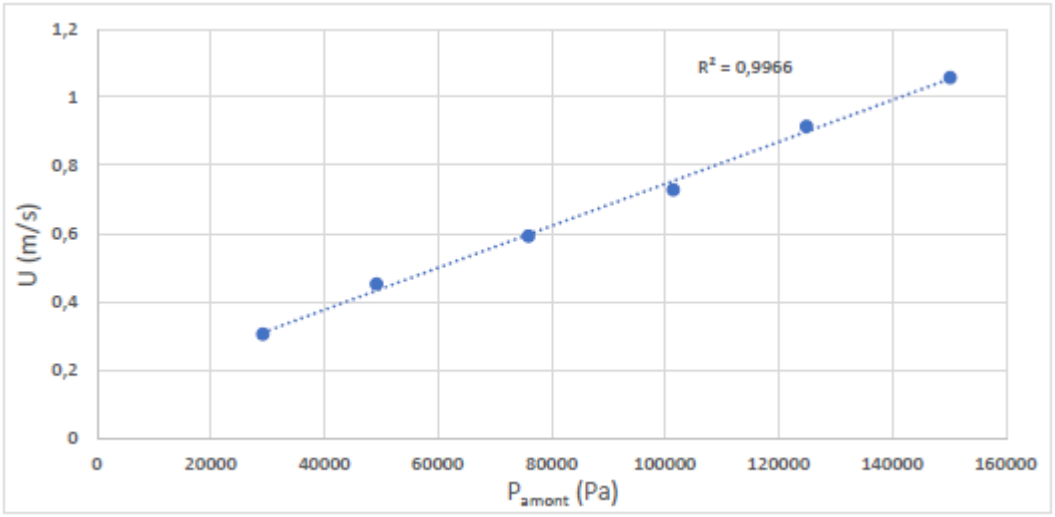

Figure 2.18. Relation between the water velocity and the upstream pressure without the pressure regulator implemented (Palut, 2021).

To determine the core offset equipment for Schlieren visualization was installed (Figure 2.19. Until this point to measure the core displacements only the high-speed camera was used, but it had a limited resolution. It was opted to implement the distance sensor since it is a non-intrusive method, and it would gain accuracy in the measurement of the core offset.

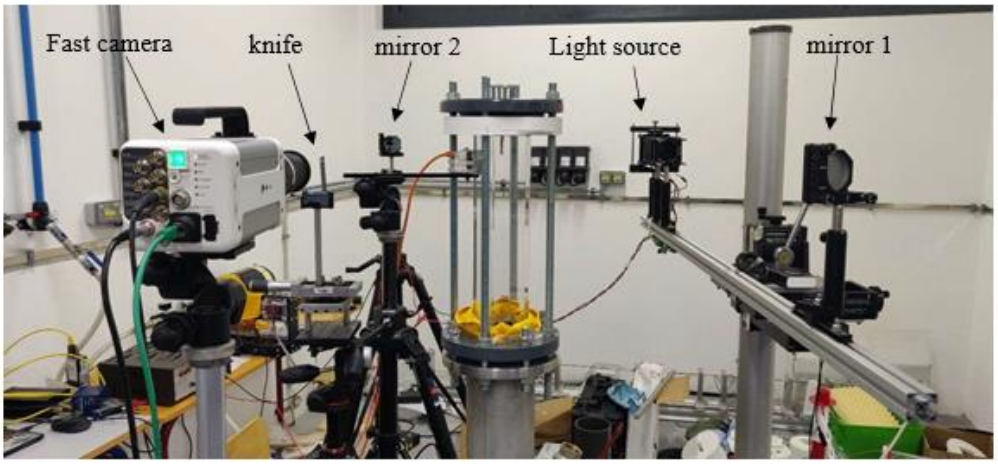

Figure 2.19. Schlieren visualization setup (Palut, 2021).

In the Figure 2.20 is shown that Axom OWLF 4007 distance sensor works by triangulation. A laser beam is sent to the object that is to be measured, in this case was the core, and the surface of the object reflects the beam that is captured by a line of photodiodes.

The sensor correlates the difference in light reflection with the position of the core, measuring the core displacement.

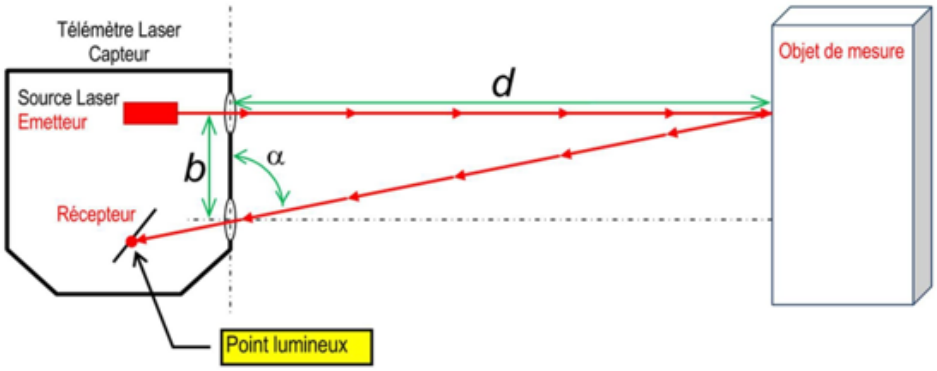

Figure 2.20. Distance sensor working schematic (Palut, 2021).

Two cores were selected by Safran to be tested, which are in decreasing order of priority: symmetrical oval core with inclination and the NACA 9320 core. For each velocity, five tests were performed, the velocities were 0.15 m/s; 0.20 m/s; 0.25 m/s; 0.30 m/s; 0.4 m/s; 0.5 m/s; 0.6 m/s; 0.7 m/s; 0.8 m/s; 0.9 m/s; 1 m/s. In this document only the results of the core displacement for the symmetrical oval core with inclination are addressed. The experiments with the NACA 9320 core weren´t done and the symmetrical oval core with inclination was the one used for the experiments done during the present internship.

In the Figure 2.21 is shown the displacement of the core according to the velocity of the water. The bars represent the standard deviation of the five measurements and the curve was proposed to model the core displacement behaviour. It's visible that with the increase of velocity the uncertainty of the offset measurements is higher. The uncertainty of these results is partly due to the turbulent state of the free surface at the moment of impact with the core, since the pressure regulator isn´t installed. For higher velocities, the formation of many bubbles due to the honeycomb is observed which also contributes to the non-repeatability of tests. A recirculation zone appears on both sides of the core and the appearance of a recirculation pocket on one side of the core, unpredictably, contribute for these displacements results. The recirculation zone may be induced by the roughness of the core.

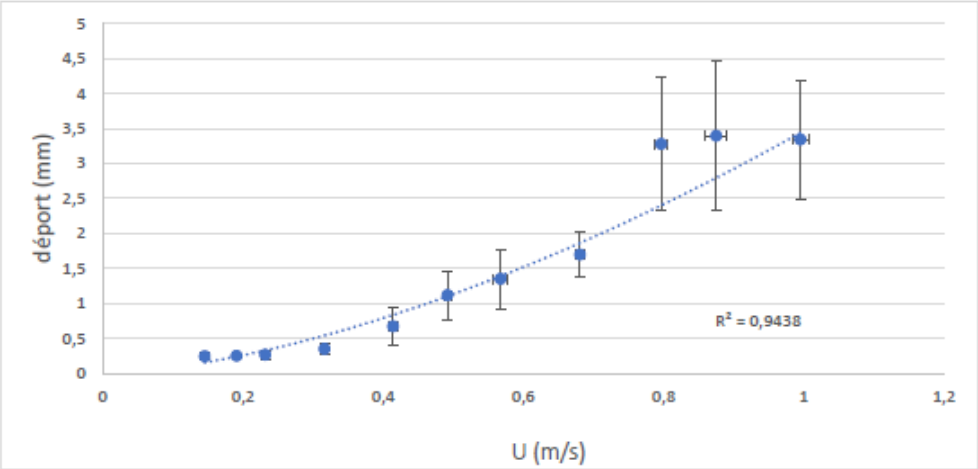

Figure 2.21. Symmetric oval core with inclination offset measurements (Palut, 2021).

In every test the visualization of the free surface was captured by the speed camera giving a better understanding of the fluid impacting the core. In the sequence of images throughout time, in Figure 2.22, is possible to observe the turbulent state of the flow, the bubbles formed and the recirculation zone.

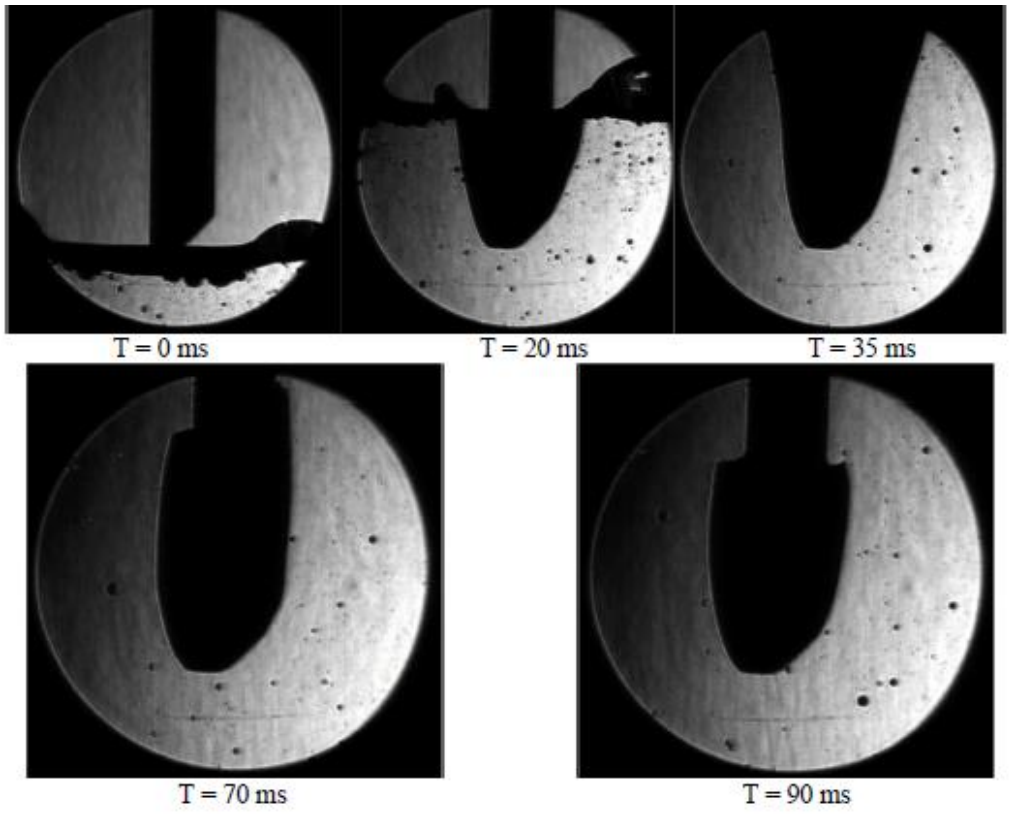

Figure 2.22. Visualization of the symmetrical oval core with inclination at $U = 0.99\ m/s$ (Palut, 2021).

2.4.3. Setup Limitations

There are several limitations in the setup that cause serious impact on the results. The pressure regulator allows the surface of water to have a constant behaviour and a better calibration of the experiment, but doesn´t permit to reach the expected impact of velocity of 1 m/s, that is necessary. The veins fabricated weren´t exactly parallel, what contributed for difficulties in visualization using the Schlieren visualization method. The height of the vein wasn´t sufficient for the stabilization of the fluid and the core to be attached to the top lid of the setup caused difficulties in the tests. The honeycomb contributed for the stabilization of the fluid, however for higher pressures is observed that there are some turbulences. In order to achieve the experimental results required was conclude that a new setup with several changes should be designed and implemented.

3. EXPERIMENTS FOR THE PRESSURE SETUP

Inquiring the range of pressures that permit to obtain 1 m/s, with a steady flow and the impact of the pressure setup in the velocity of the fluid were the goals of these experiments. It was of great interest to perform some experiments to get a practical knowledge of the setup and to confirm the results obtained with and without the pressure regulator.

3.1. Experimental methodology

As mentioned in subchapter 2.2 the experimental setup is composed of several parts. The pressure setup is formed by several equipment, it begins with a pressurized air network, connected to an air tank with a pressure reducer. This air tank is connected to the water tank of the setup with several tubes. Between the tanks there are a pressure sensor and a pressure regulator. The pressure regulator and the upstream pressure sensor are connected to a controller that is connected to a computer where a program was developed in LabView.

The program allows the automated acquisition of data, from the pressure sensor upstream and the pressure sensor in the water tank. The acquisition of data of the pressure sensor in the water tank is possible due to a data acquisition device (DAQ) that is also connected to the computer.

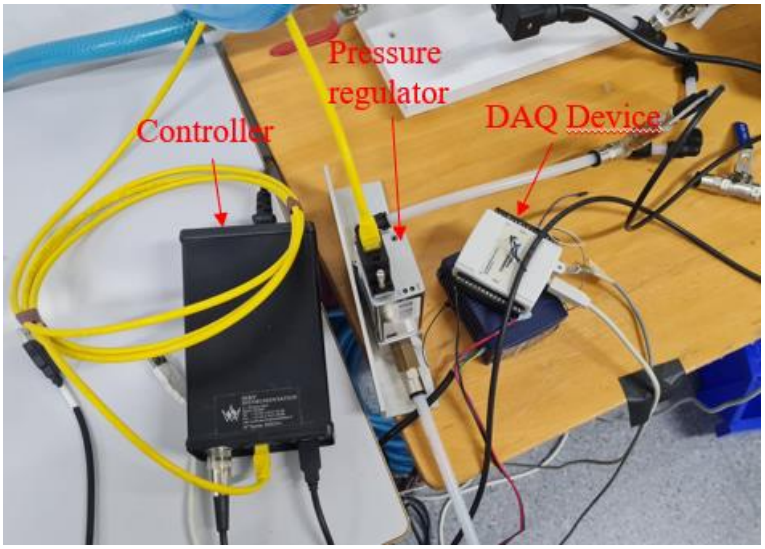

Figure 3.1. Elements of the pressure setup

This allowed the implementation of a camera trigger when the fluid reaches a certain pressure (parameter in the programme developed in the Labview), hitting the core. The video and images recorded only correspond to the instants between opening and closing the manual valve, this way the data from each test has the same duration.

The circuit of pressure ends in the metal tank, where a manual valve is in the wall of the water tank. While this valve is open the tank is at the atmospheric pressure and the air that comes from the circuit of pressure is released by the valve. However, when the valve is closed the internal pressure in tank increases and the water rises in the vein. When the water reaches the core, the valve is opened releasing the air contained, causing the water to go down back to the metal tank. For each test, after setting up the pressure circuit closing the valve and open the valve determine the beginning and the ending of the test.

The pressure upstream in the air tank and the pressure in the metal tank, were the two parameters measured in the three tests made at 1m/s. The speed camera recorded the flow reaching the core.

3.2. Results and data analysis

To establish a calibration of the setup with and without the pressure regulator, several experiments were done. The latest results obtained were analysed and was observed that for 1.4 bar of upstream pressure without the pressure regulator a velocity of 1 m/s was achieved. To have a better understanding of the impact of the pressure setup on the velocities achieved and the behaviour of the fluid, three new tests were done with and without the pressure regulator for a pressure of 1.4 bar.

The two methods for calculating the velocity, mentioned in chapter 2.3.2, of water had a difference of 2% in the results (Palut, 2021). For time consuming reasons and since the two methods show to be valid was chosen the equation (2.2), to determine the ascendant flow velocity of water.

The data of three tests concluded that the velocity achieved using the pressure regulator (Figure 3.2) corresponds to the previous results. For an upstream pressure of 1.4 bar, a velocity between approximately 0.15 m/s and 0.16 m/s was expected. However, the results obtained without the pressure regulator were not similar to the previous results, instead of a pressure of 1.4 bar, the sensor measurements indicated 0.9 bar. Additionally, for an upstream

pressure around 0.9 bar a velocity of 0.57 m/s to 0.62 m/s was achieved (Figure 3.3), when a velocity around 0.7 m/s was expected. As mentioned in chapter 3.1, the pressure sensor upstream and the pressure regulator are connected to the controller, this piece of equipment was turned off for the tests in which the pressure regulator was not used. Consequently, the measurement of the pressure given by the upstream sensor doesn´t correspond to the real upstream pressure of 1.4 bar.

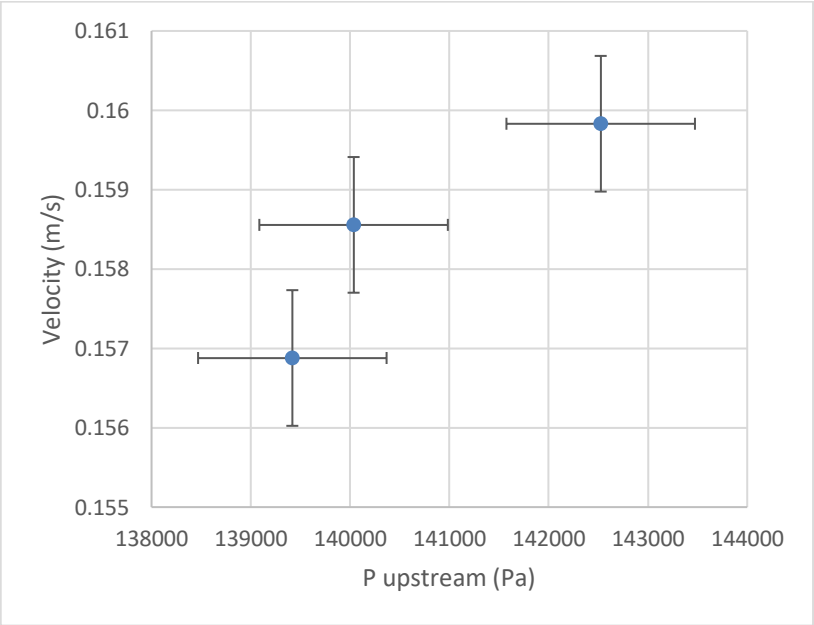

Figure 3.2. Relation between the velocity and upstream pressure for three tests with the pressure regulator.

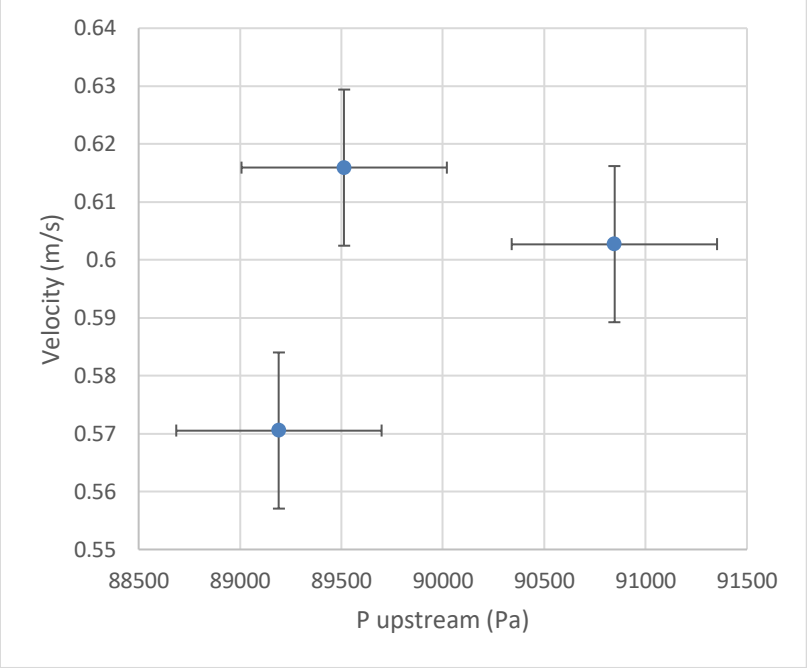

Figure 3.3. Relation between the velocity and upstream pressure for three tests without the pressure regulator.

In the Figure 3.4 and Figure 3.5 is notorious the impact of the pressure regulator on the behaviour of the fluid. With the pressure regulator the fluid shows a free surface more stable, however yet with some fluctuations. The appearance of bubbles caused by the honeycomb is unpredictable and they are visible at the moment of impact with the core. The vein has not enough height for the fluid to become stabilized and uniform. Without the pressure regulator the free surface shows to be turbulent with a lot more fluctuations and bubbles, similar to the Figure 2.22. A recirculation zone around the core after the impact is visible. The acquired images by the high-speed camera have a resolution of 1024×1024, the acquisition frame rate was of 1000 fps.

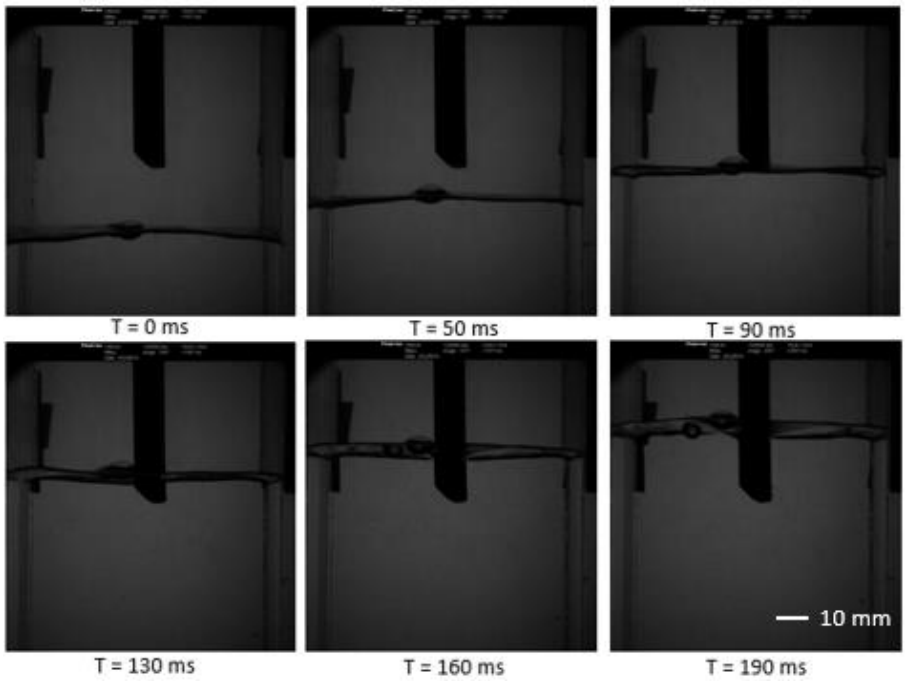

Figure 3.4. Visualization of the symmetrical oval core with inclination with pressure regulator.

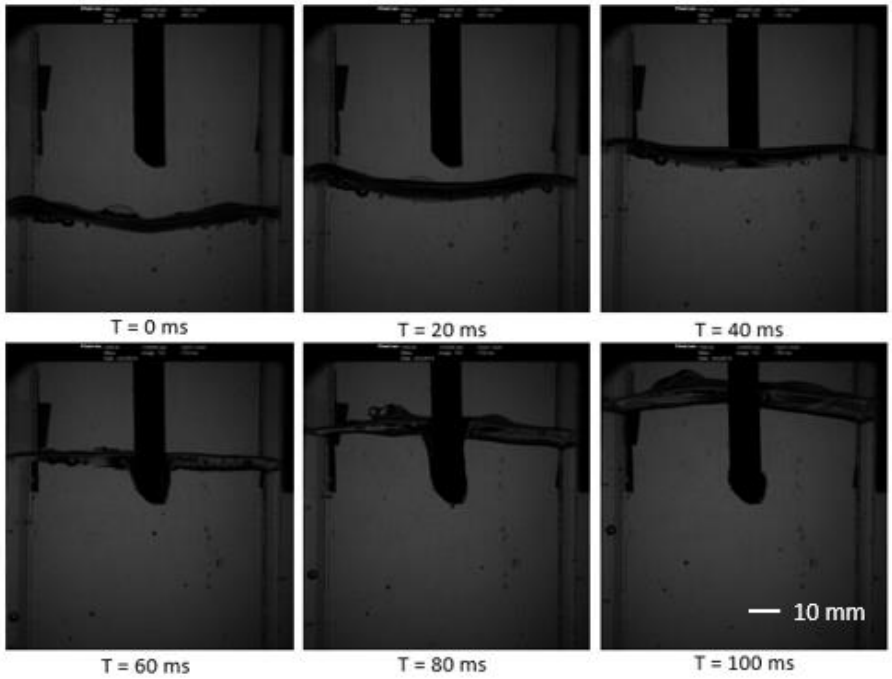

Figure 3.5. Visualization of the symmetrical oval core with inclination without pressure regulator.

4. IMPROVEMENT PROPOSALS

With the realization of the experiments, mention in the previous chapter, it was possible to observe the setup functioning and to understand the difficulties encountered previously. In addition to the problems mentioned in the subchapter 2.4.3, it was observed that while doing the tests, several parts in the setup were not correctly attached what cause leakage in several parts of the setup. The manual valve that is activated to stop the water from continuing raising, for higher velocities, becomes hard to handle which causes the water leakage on top of the setup. Several pieces were not full attached with nuts what causes the vein to raise up from its original position for higher velocities. The quantity of water in the tank is not replaced after each set of tests. For higher velocities it was possible to hear the shortage of water in the bottom of the metal tank. The top attachment part of the setup is 3D printed and it proved to be fragile since it was broken, and it does not have plane surfaces which causes accommodation difficulties in the setup. The honeycomb presented should be improved, being that, for higher velocities can contribute to achieve a steady free surface. The attachment piece located in the middle of the setup has an internal piece (Figure 4.1) with a variable section that constrains the fluid from a circular area of 17.67×10^{-3} m^2 to a square area of $6.4 \times 10^{-3} m^2$ This obstacle and the honeycomb contribute to a significant change in the behaviour of the fluid when reaches the vein. Since the experiments performed confirm that the setup needs several improvements to achieve the desired goals, numerous changes are proposed in this chapter. Different parts were designed with the CAD software Autodesk Inventor, Appendix B contains the dimensions and specifications for all the designed parts.

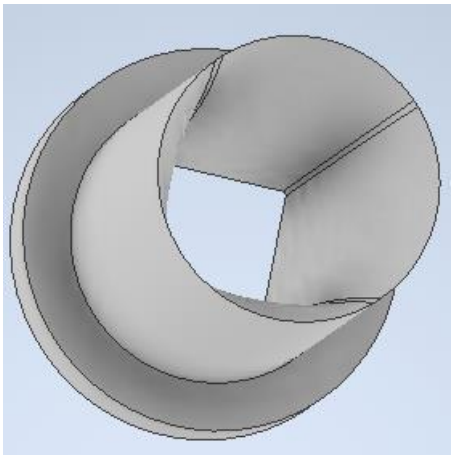

Figure 4.1. Part with convergent section.

4.1. Parts Designs and equipment selection

The path of the fluid should have a constant area to improve the results obtained so far. In order, to achieve this, a piece was designed (Figure 4.2) to put inside of the tank with square shape interior with an area of 6.4×10^{-3} m^2, corresponding to the internal area of the vein.

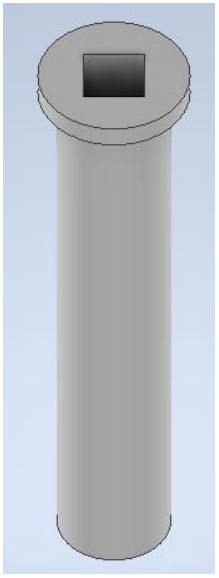

Figure 4.2. Internal part that is placed inside the metal tank.

Having in consideration the improvements in the behaviour of the water flow obtained using the honeycomb, a new design was done and was suggested the addition of a new honeycomb (Figure 4.3, (a)) to be placed in the bottom of the internal piece inside the tank. The results, by Palut, 2021, show that having a smaller height can improve the behaviour of

the water flow. However, having in consideration the results obtained by Loehrke and Nagib, 1976 is proposed to have a cell size and a height that respect the equation (4.1) , where l corresponds to the length of the honeycomb and M to the diameter of the cell size.

$$\frac{l}{M} \geq 10 \tag{4.1}$$

The cell size suggested is of 0.5 mm and the height of the honeycomb is of 5 cm. The wall thickness desired is of 0.15 mm. A wall of 0.7 mm thickness was designed around the honeycomb, something that the previous ones printed did not have, to give some support to the extremities.

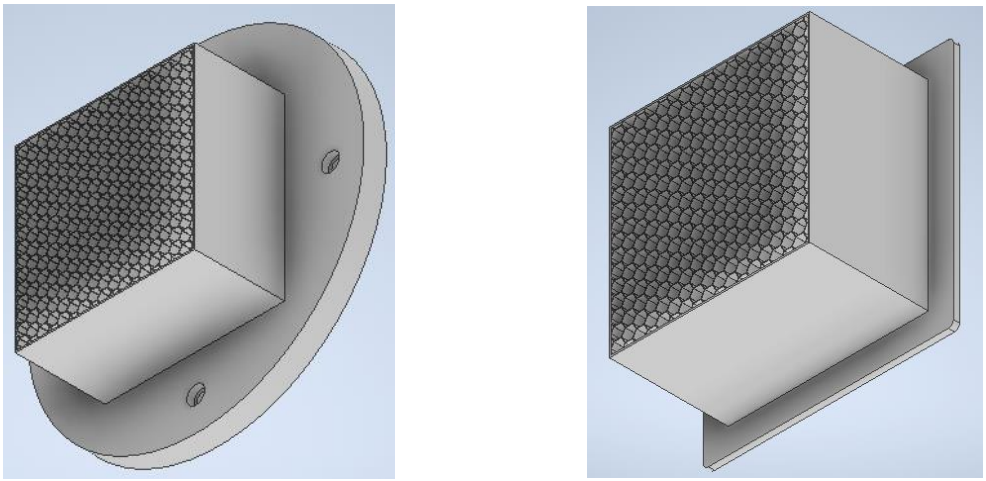

(a) (b)

Figure 4.3. (a) Honeycomb placed in the bottom of the internal part.; (b) Honeycomb placed in the bottom of the vein.

The experimental setup was assembled for the experiments done referred in chapter 3 and it was observed that different attachment parts were used between the top of the tank and the vein. In order to minimize the quantity of parts, promote a better attachment and stop water leakage from between the parts, a unique part (Figure 4.4) was designed bringing together the top of the tank, the vein, the internal part inside the tank and the honeycomb.

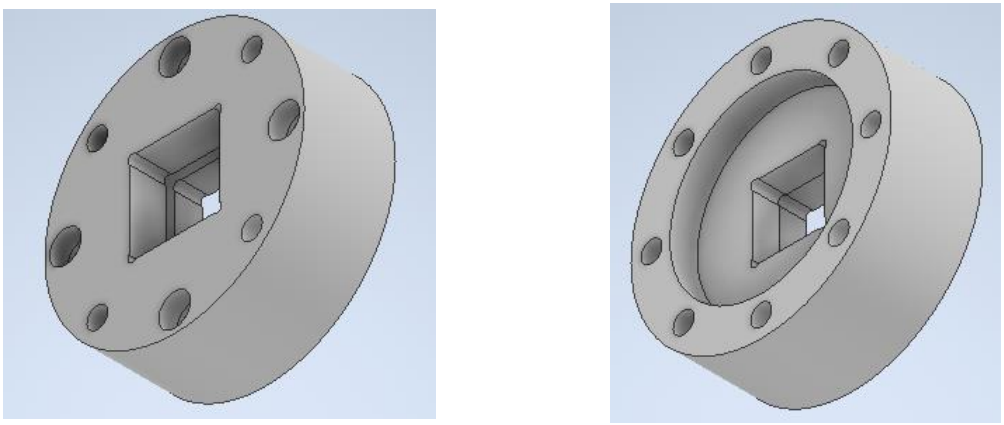

(a) (b)

Figure 4.4. (a) Top of the attachment part; (b) Bottom of the attachment part.

Without the internal part that constrains the fluid and the implementation of the internal piece inside the metal tank, the fluid will have a path with a constant section until reaching the core. The two honeycombs are the two parts in the path of the fluid. A vein with a bigger height was design to allow the stabilization of the flow after the second honeycomb. Additionally, this higher vein would allow the water flow to continue after the core without interference, provided that the core is placed in the middle of the vein. This vein has a height of 900 mm and a wall thickness of 10 mm. The vein should be produced in a transparent material to facilitate the visualization methods, it is recommended plexiglass. A reduction of the wall thickness will allow a vein with less weight, since the ones used are extremely heavy and a better visualization of the flow using the schlieren visualization. The indication that the walls need to be parallel with a high level of accuracy needs to be given to the manufacturer, since two of the veins fabricated did not have this characteristic and have prevented the use of Schlieren visualization.

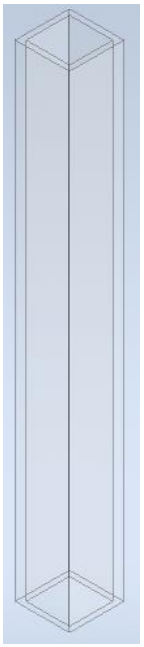

Figure 4.5. Plexiglass vein.

A piece where the core could be attached to (Figure 4.6) was designed, to allow the core to be in a position inside the vein where the phenomenon of the displacement of the core could be studied, without the contact of the water with the top attachment piece of the setup. This support piece has an aerodynamic design to fit perfectly inside the vein and not to disturb the fluid after reaching the bottom of the core. In the middle of the piece a rectangular hole with circular corners allows the core to be screwed with a 40 mm long M5 bolt. If the core is screwed tightly results similar to the obtained until now are expected, since in the present setup the core is firmly attached to the top lid. The core will be able to have a sliding movement in y-axis (horizontal movement) and z-axis (vertical movement) if it is screwed with some slack. It is important to know if the results and the behaviour of the flow are affected when the core is attached with slack. If that is the case, Safran can correct its moulds and prevent more defects on the blades produced. The core support piece in its four corners has 4 threaded beams connected to the top lid using a total of eight $M10 \times 1.5$ nuts.

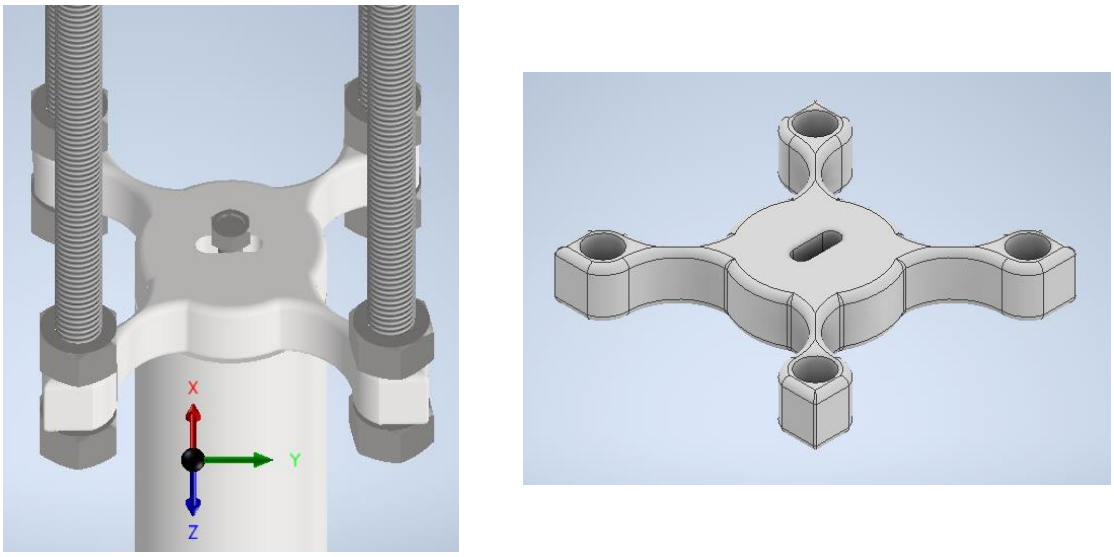

(a) (b)

Figure 4.6. (a) Core support piece installed in the vein. (b) Core support piece.

The top part of the setup (Figure 4.7) was designed with holes for accommodation of the threaded beams and it is open to the atmosphere. The previous top piece of the setup and the honeycombs were 3D printed. The pieces turned out to be fragile, with rugosities and with size limitations. Therefore, it is recommended that 3D printing should not be used for the fabrication of the pieces. Additionally, the recommended material for the fabrication of all the pieces designed is a polymer, like PVC.

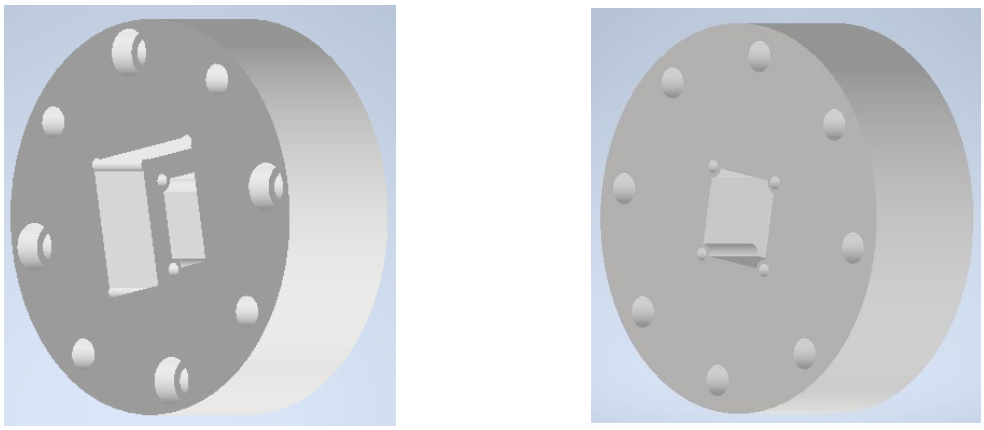

(a) (b)

Figure 4.7. (a) Bottom of the top piece; (b) Top of the top piece.

To understand if the capacity of thirty litters of the tank would be enough to the new dimensions of the setup, calculations were done. The volume (4.2) is defined by:

$$V = A \times L = 0.0064 \times 1.7607 = 0.0112\ m^3 \quad (4.2)$$

Being that A corresponds to the internal area of the setup, L to the height from the bottom of the internal piece to the top piece of setup. The value of volume corresponds to $11.2\ l$, which does not exceed the volume of the tank and for that any change is require to the tank.

A new ceramic core (Figure 4.10 (a)) was delivered by Safran and since the setup did not have the right accommodation to perform the tests, a new attachment piece was designed. The new attachment piece (Figure 4.10 (b)) is similar to the one design for the other cores, however it has a rectangular hole in the bottom of the piece for the entrance of the core and a circular hole on the top for the accommodation of the head of the core. A circular plate fits on the bottom of the piece and four M3 $\times$ 6 screws are used for the attachment.

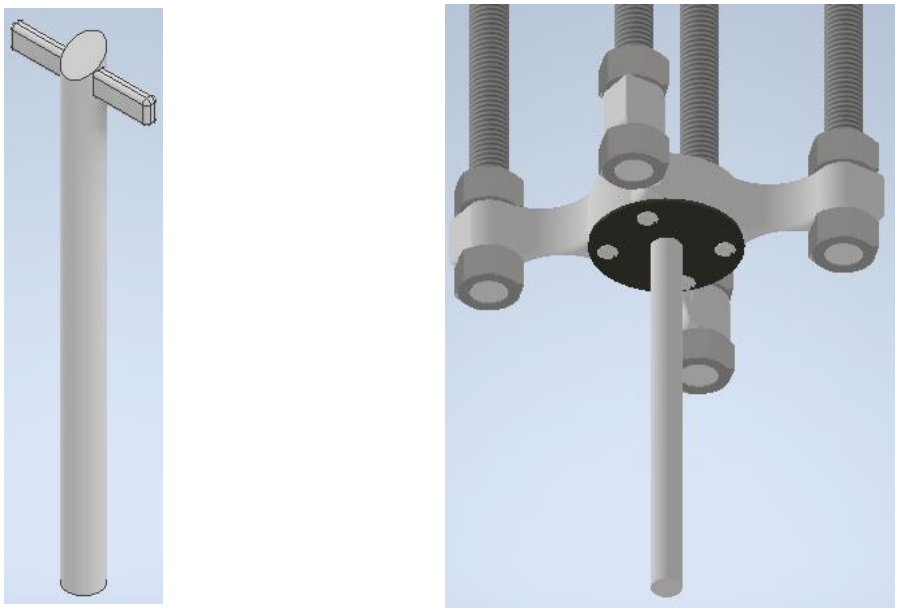

(a) (b)

Figure 4.8. (a) Ceramic core.; (b) Core support piece adapted to the ceramic core.

To achieve a velocity of 1m/s and a state of the fluid where the free surface is steady and without any perturbation, apart from the new pieces necessary, improvements in the pressure setup are needed. The current pressure regulator does not operate in the range of

pressure necessary, being the change of this piece of great importance. An approximate extrapolation, with the experimental results of Palut, 2021, was done to decide the range of pressures the pressure regulator should have to achieve the proposed goals. The data of the experiments was not available, the Figure 2.17 was the only resource for the approximate selection of three points. In Figure 4.9 is observed that the new pressure regulator should have a minimum value of 12 bar if a velocity of 1 m/s is desirable. The regulator implemented in the setup is from Brooks® Instrument and it's from the series SLA5800. The regulator suggested is from the same company and it´s the model SLA5810. This pressure regulator has a range of pressure operating from 1 psi to 1500 psi (approximately 0.07 bar to 103 bar).

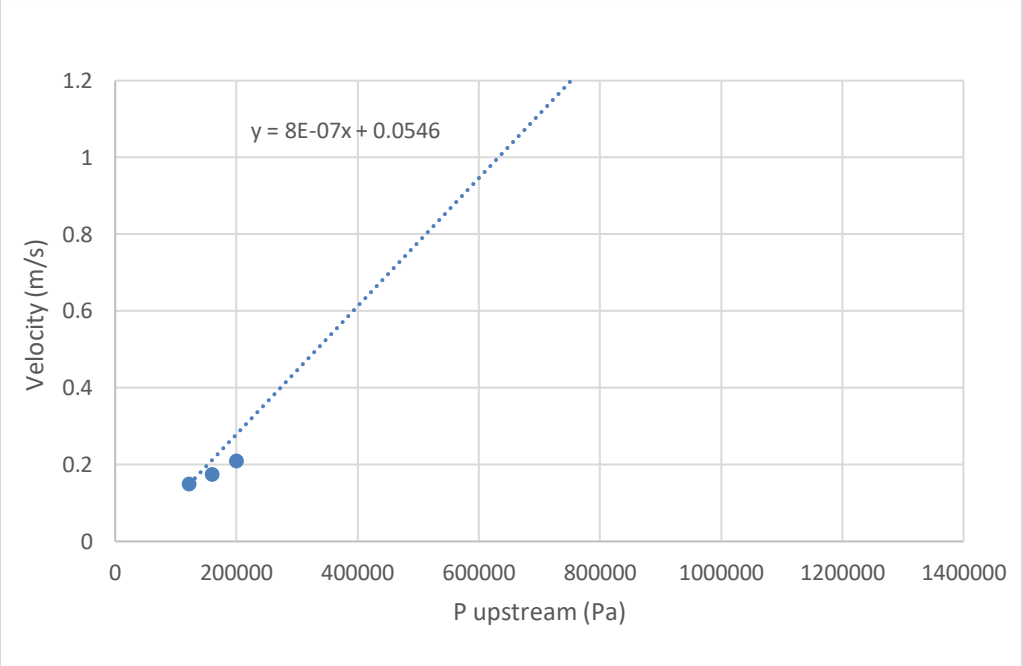

Figure 4.9. Extrapolation of the relation between velocity and upstream pressure.

The air network to which the pressure setup is connected has a maximum pressure value of around 7 bar. Since a higher pressure is required the implementation of a pressure regulating table is suggested, this table compresses the air until the required value. Several pieces of the setup have a maximum operation pressure value. The specifications catalogues of the sensor in the tank and of the several tubes and connectors show that these don't support the value of pressure necessary on the setup. These pieces would also need to be upgraded.

To improve the efficiency of the water shutdown at certain height, without needing the manual valve, the implementation of a 5/2 solenoid valve is suggested. The valve is from

Asco™Numatics, series 521, with a differential return operator. The valve would be controlled by the program done in the LabView that controls and collects other data of the setup. The valve's trigger would have the same working mechanism as the trigger of the camera, through the DAQ.

The water leakage on top of the setup, for higher velocities, could damage the equipment around the experiment. The implementation of the pieces and equipment mentioned so far, as the core being positioned in the middle of the vein and the implementation of the solenoid valve prevent this situation from happening. However, for safety reasons it is suggested a safety system, where if the solenoid valve does not work the water will be directed to a place that would not cause damages. The system is composed of two tubes, one with 300 mm and the other one with 1700 mm, two elbows, being that these four elements have a 50 mm diameter, a piece with the fitting for four screws to firmly attached the safety system to the top of the experimental setup and a reservoir placed on the floor.

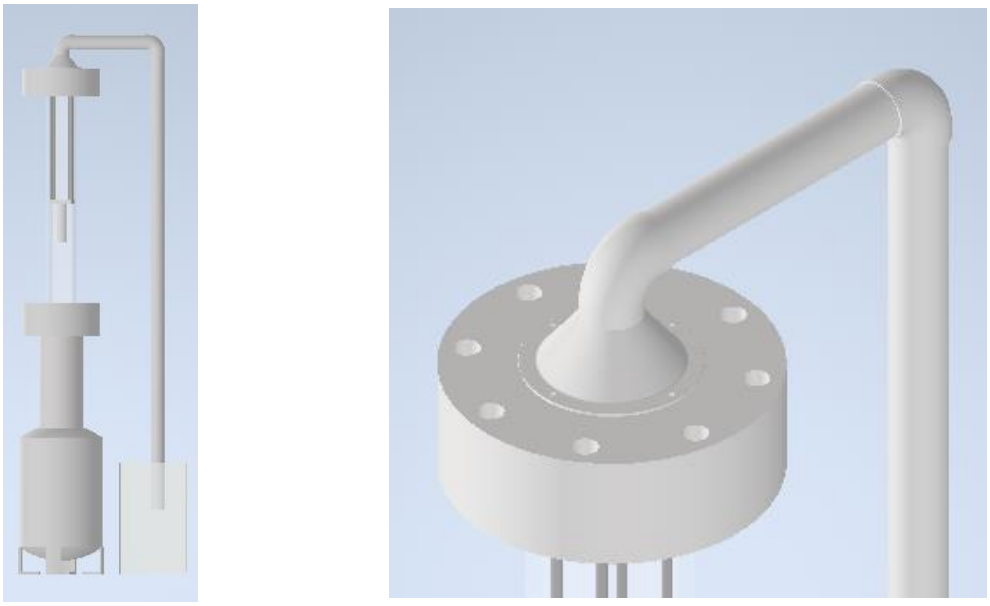

(a) (b)

Figure 4.10. (a) Experimental setup with the safety system.; (b) Detail of the safety system.

5. SIMULATIONS

Different simulations were done to evaluate distinct aspects of the setup. These were to understand if the fluid rising at a velocity of 1 m/s at a higher upstream pressure of 12 bar would cause any structural impact in the vein, but also to evaluate several parameters when the fluid encounters the honeycomb and the core.

5.1. Structural analysis of the vein

The changes suggested to implement involved different parts of the setup. The improvements in the pressure setup promoted the modification of several pieces. A structural analysis simulation studying if the vein would not suffer any type of drastic structural change was done, being that the upstream pressure suggested is ten times higher than the one normally used for the tests. The software used was Abaqus FEA, a program of finite elements analysis. In this software the user is the one who is responsible for the units of the parameters inserted, this is something to take in consideration to do a right evaluation of the results. As such, the international unit system was considered. The vein was exported to the software in meters and the properties of the plexiglass used were: 3200000000 Pa of Young's Modulus, 0.35 Poisson's ration and 1190 kg/m^3 of mass density ('The Engineering ToolBox'). The pressure located in the four inside walls of the piece was defined by the equation (5.1), in which the pressure in the coordinates (0,0,0) is given by the pressure applied to the water plus the pressure generated by the weight of the water inside of the vein and in the coordinates (0,0.9,0) is 0 Pa. Additionally, P corresponds to the pressure in the wall and y to the height of the vein. The gravity was applied in all the structure.

$$P = -1 \times 10^6 \, y + 1 \times 10^6 \; [Pa] \tag{5.1}$$

The boundary conditions for the surface extremities of the vein were considered to be embedded. The results show that the highest value for the Von Mises Stress is of 12.99 MPa (Figure 5.1). The value of the Tensile strength for acrylic is of 70 MPa, thus the augmentation of the upstream pressure will not cause a severe structural change in the vein. The values of deformation also confirm this, being that the highest value of deformation in the vein is of

6.090×10^{-4}m (Figure 5.2). The present figures have an exaggerated augmentation of the vein walls, being that a deformation scale factor of $+1.478 \times 10^{2}$ was used.

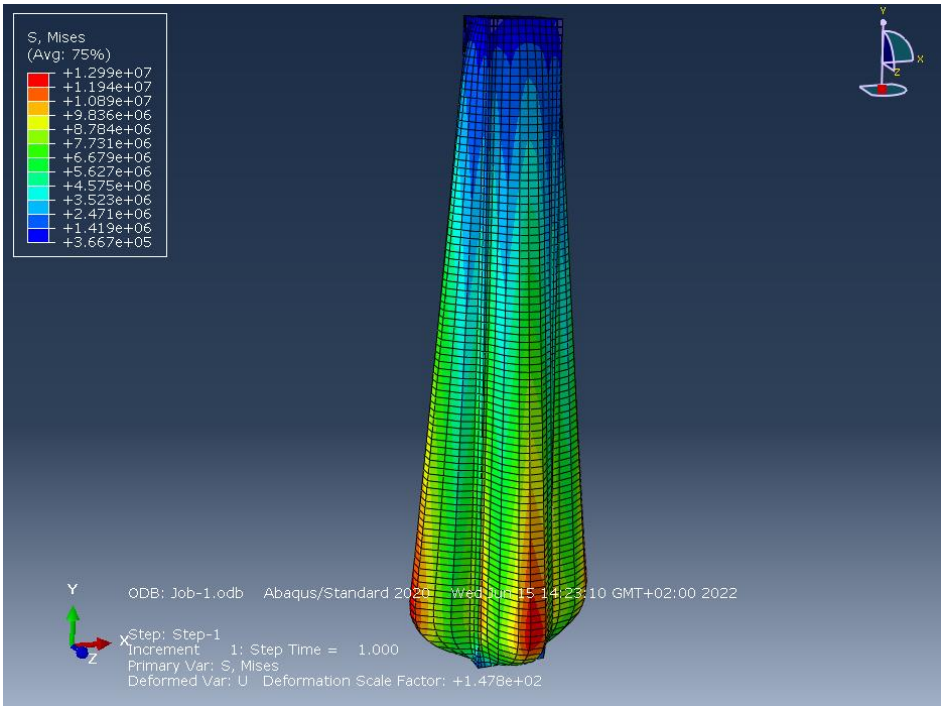

Figure 5.1. Von Mises Stress in the vein.

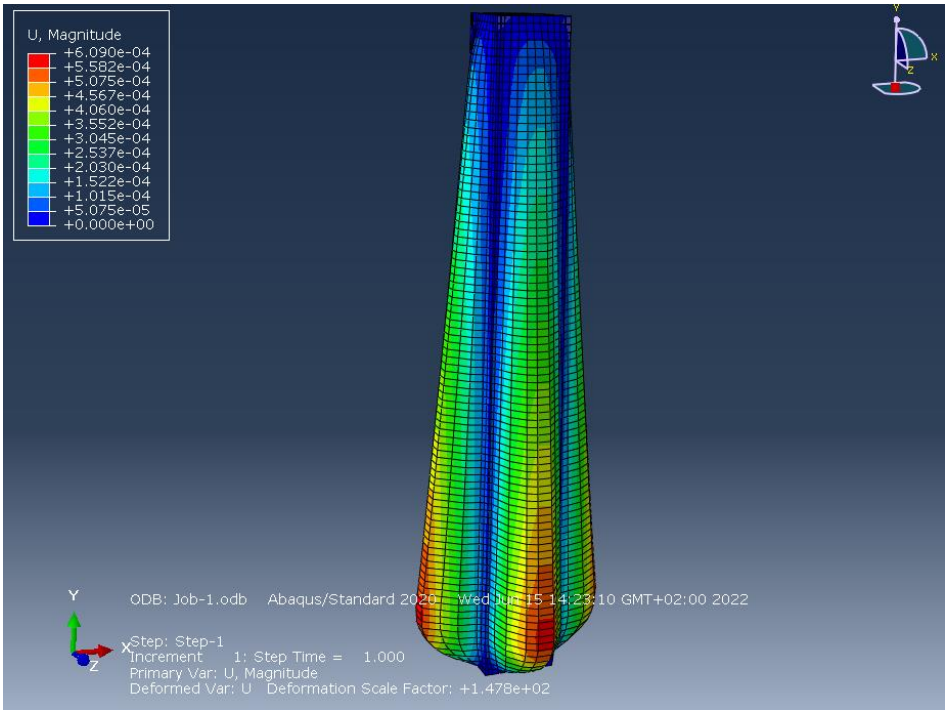

Figure 5.2. Deformation of the vein.

5.2. Fluid dynamics in the honeycomb and core

In the previous project study, a further comprehension wasn´t addressed, beyond the experimental results, of the interaction of the fluid with the different internal pieces of the setup, in particular the honeycomb and the core. It was concluded that the implementation of the honeycomb would be an improvement if implemented with optimized dimensions and under the right conditions. It was evaluated if the pressure loss provoked by this component was significantly but was conclude by calculations that this loss wasn´t relevant.

The pressure at the tip of the core, when impacted by the water, was not measured. This parameter is important to be known to choose an ideal attachment for the core, having in consideration the movement that is expected.

The software Simcenter STAR-CMM+ was used to run several simulations. The STAR-CMM+ is a Finite Volume software based on computational fluid dynamics. It permits modelling and analysis of a large range of problems. The block that represents the interior of the vein and the core were designed in the software and the honeycomb was imported (Figure 5.3). A subtraction boolean operation was made, where to the block created, the core and the honeycomb were subtracted, this element, from now on called subtract, represents the fluid inside the vein.

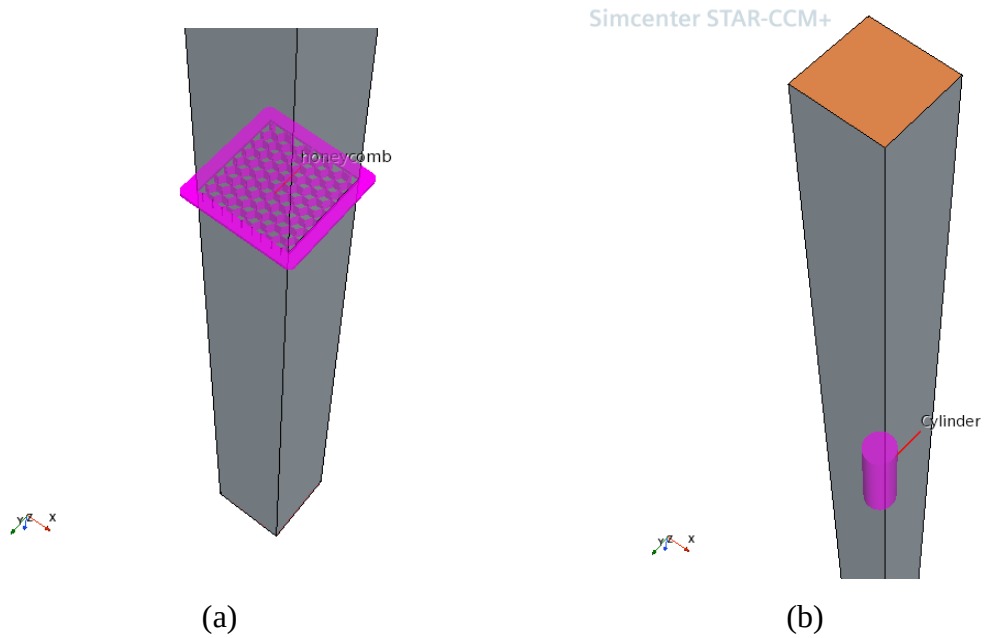

(a) (b)

Figure 5.3. (a) Geometrical scene detail of the honeycomb.; (b) Geometrical scene detail of the core.

Each surface of the subtract was defined as a boundary in the menu Regions (Figure 5.4 (a)). The surface bottom, left, right and top were defined as walls, the inlet as velocity inlet and the outlet as pressure outlet.

In Operations was chosen the option of automated mesh for the generation of the mesh (Figure 5.4 (b)). The Meshers selected were Surface Remesher, Polythedral Mesher and Prism Layer Mesher. The Polythedral mesher was selected because this type of mesh is easy and efficient to build. The Default Controls menu has been altered by consulting the official STAR-CMM+ Help forum and by acquiring a certain sensibility for the values of the parameters after some trials and errors. A comprehensive exposition of the used values and images of the meshes are presented in the Appendix A.

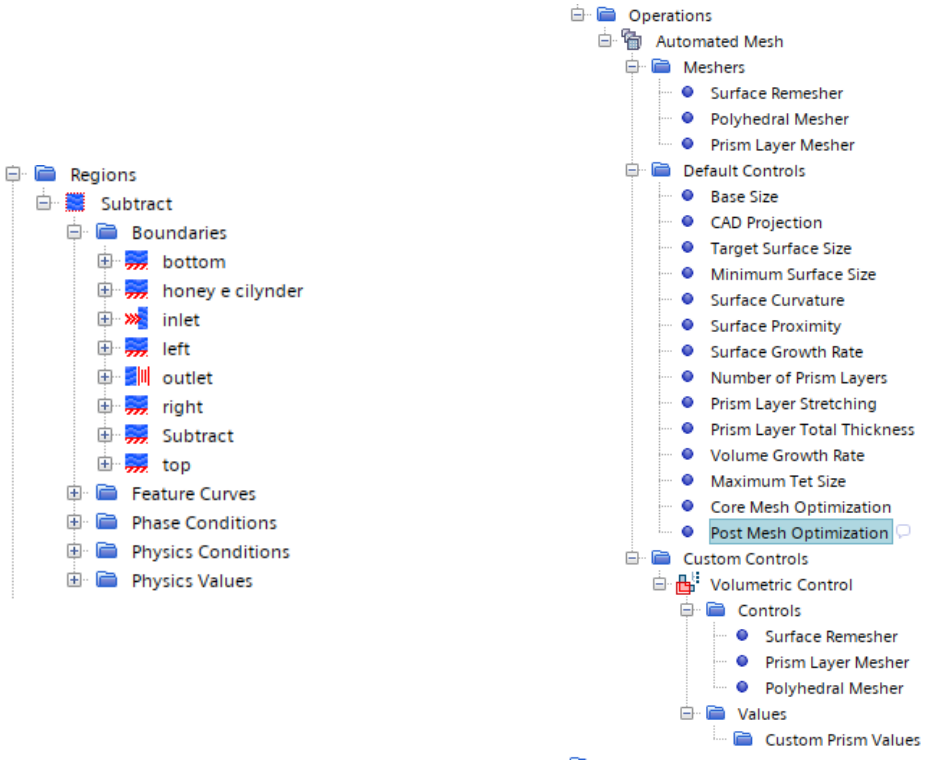

(a) (b)

Figure 5.4. (a) Regions Menu.; (b)Operation Menu.

5.2.1. Steady flow simulations

Steady simulations were performed with the goals of evaluating if the honeycomb caused any restrictions to the fluid and to gain acquaintance with the software, for future more complex studies.

Numerous specific parameters were changed in the menus of the simulation. In the Stopping Criteria menu, the number of the Maximum Steps chosen was of 1000. Several simulations were run to conclude that the value for the Number Prism of Layers that had the best performance was eight, having as a reference the convergence of the residuals. The selected models are present in Figure 5.5, the K-Epsilon Turbulence was chosen, because it provides a good compromise between robustness and accuracy. The model Liquid was selected being that the only fluid present in this simulation is the water. The initial conditions (CFD | Autodesk Knowledge Network') altered were:

- Turbulence intensity with the value of 0.05
- Turbulence viscosity ration with the value of 10
- Velocity with the value of (0,0, -0.5) m/s

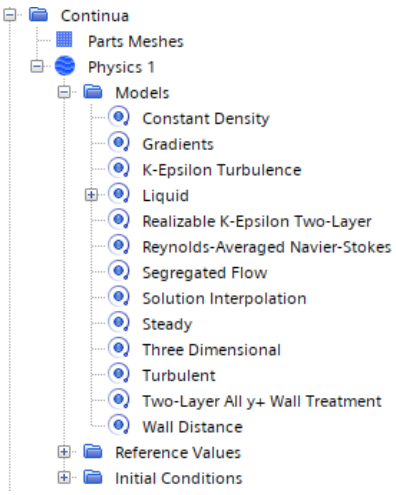

Figure 5.5. Models selected for the steady flow simulations.

In the Figure 5.6 and Figure 5.7 is possible to see a scalar scene of a plane section with the coordinates (0,1,0) m, where the velocity parameter is shown. The velocity in the surroundings of the honeycomb is approximately 1 m/s and is observed that pressure drops exerted by this component does not significantly influence the magnitude of the velocity. In the sides of the core is observed that the velocity increases, reaching 1.54 m/s and at the top

and bottom of the core the velocity is considerably smaller reaching the value of 0.00199 m/s.

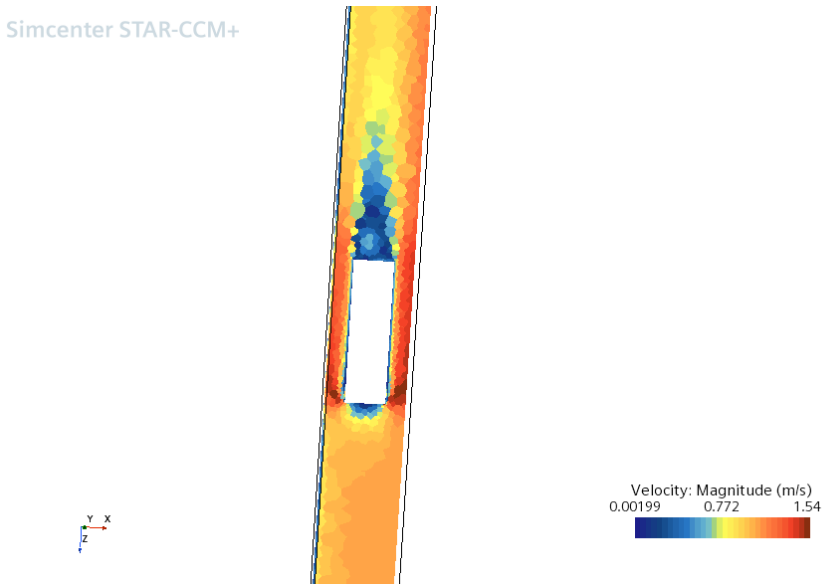

Figure 5.6. Scalar scene of the velocity in subtract in steady simulations. Detail in the surroundings of the core.

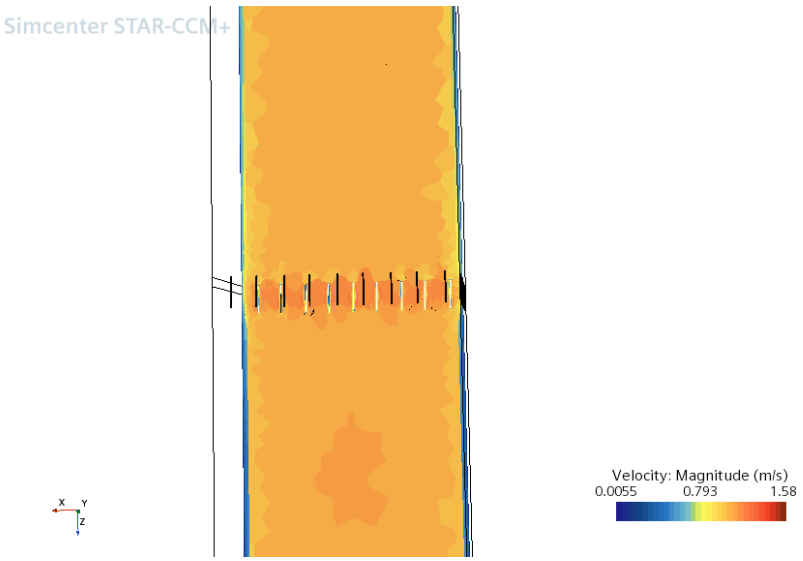

Figure 5.7. Scalar scene of the velocity in subtract in steady simulations. Detail in the surroundings of the core.

The Force was a parameter calculated and corresponds to the pressure being applied in different parts of the Subtract (Figure 5.8). Experimentally this values weren´t measured and therefore a validation of these results is not possible, however this simulation provided

a reference value. The Force applied in the honeycomb is of 0.275 N and in the core is of 1.21 N.

```
Component in direction: [ 0.000000e+00,  0.000000e+00, -1.000000e+00] in Laboratory coordinate system
Part             Pressure (N)  Shear (N)     Net (N)
---------------- ------------- ------------- -------------
bottom           -3.160099e-17  3.479111e-01  3.479111e-01
Cylinder Surface  1.213216e+00  1.140975e-02  1.224626e+00
honeycomb         2.753501e-01  2.177856e-01  4.931357e-01
inlet            -3.340535e+00  0.000000e+00 -3.340535e+00
left             -1.078570e-16  3.485078e-01  3.485078e-01
outlet            0.000000e+00  0.000000e+00  0.000000e+00
right            -1.731078e-16  3.545987e-01  3.545987e-01
top              -6.838079e-17  3.486997e-01  3.486997e-01
---------------- ------------- ------------- -------------
Totals:          -1.851969e+00  1.628913e+00 -2.230559e-01

Monitor value: -0.2230559327503474
```

Figure 5.8. Magnitude of the Force in each surface for the unsteady simulation.

5.2.2. Multiphase unsteady flow simulations

A more complex numerical study was performed, to simulate the closest scenario possible to the experimental reality, using an unsteady flow while having present two phases: water and air (multiphase model). However, is important to address that the simulations done do not correspond to the reality, because of the turbulence model used. The turbulence model adopted is the Reynolds-Average Navier-Stokes Turbulence Model (RANS), which just permits to model large-scale eddies, contrary to the Large Eddy Simulations (LES) that models the smallest eddies and Direct Numerical Simulations (DNS) that models all the scale of eddies until to the Kolmogorov Scale.

In the Stopping Criteria menu of the simulation was defined as Maximum Inner Interactions the value of twenty, after several values been ran and being noticed that the parameter Force was converging for this value. The Force parameter was followed through the simulation as other parameters like the velocity and volume fraction of water, and it was noticed that in the Force monitor plot for the first iterations with the value of twenty for the Maximum Inner Interactions the force was stabilizing, meaning that for each time step the value of the Force was converging.

For the Maximum Steps the value of 2500 was enough to achieve convergence, being that the height of the subtract is of 2.5 m, the initial velocity selected was of 1m/s and the time step used is of 0.001s.

In the multiphase unsteady simulations, the implementation of a Volumetric Control in the mesh around the honeycomb with a Number Prism of Layers of 4 was necessary in order to run the simulation without errors.

The chosen Models can be observed in the Figure 5.9, the Implicit Unsteady model was the one selected being that was the most adequate for this case. The Volume Fluid Model (VOF) being that is suited to simulate flows with an interface between the phases of the mixture (free surface flows). A Volume Fraction was implemented with two fluids the air and water, the water situated in the inlet and the air at the outlet. The initial conditions were maintained the same as in the steady flow simulations.

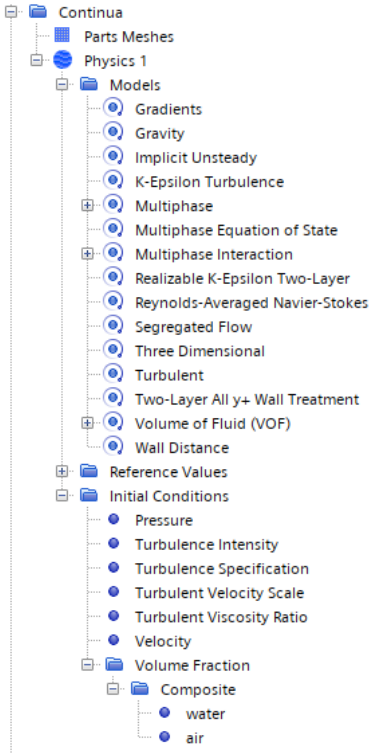

Figure 5.9. Models selected for the Multiphase unsteady flow simulations.

The final velocities reached in this simulation were very similar to the velocities achieved in the steady simulations. The Force in the honeycomb has the value of 0.335 N and the value of the Force in the core is of 2.84 N (Figure 5.10). The Force delivered in the by the impact of the water is more than two times higher than the steady flow simulations. The value of this Force has the potential to confer vertical movement to the core.

```
Component in direction: [ 0.000000e+00,  0.000000e+00, -1.000000e+00] in Laboratory coordinate system
Part             Pressure (N)  Shear (N)     Net (N)
---------------- ------------- ------------- -------------
bottom            1.613985e-16  0.000000e+00  1.613985e-16
Cylinder Surface  2.847347e+00  6.905590e-03  2.854253e+00
honeycomb         3.353317e-01  2.215176e-01  5.568492e-01
inlet            -1.589467e+02  0.000000e+00 -1.589467e+02
left             -3.312201e-10  0.000000e+00 -3.312201e-10
outlet            0.000000e+00  0.000000e+00  0.000000e+00
right            -1.076109e-14  3.323247e-01  3.323247e-01
top               1.128891e-15  3.315253e-01  3.315253e-01
---------------- ------------- ------------- -------------
Totals:          -1.557641e+02  8.922731e-01 -1.548718e+02

Monitor value: -154.87178421663955
```

Figure 5.10. Magnitude of the Force in each surface for the unsteady simulation.

6. CONCLUSION

The aim of this dissertation was the improvement of the results obtained, through the information available of a previous study and experiments. The experimental setup was not able to reach velocities in the order of m/s due to several present difficulties. In order to evaluate the impact of the pressure setup in the achievement of higher velocities, new experiments were performed.

The study of the setup and the results of the experiments conducted during this internship concluded that several changes should be implemented if higher velocities are to be achieved. Several pieces were designed for the substitution of others as well as new ones to be added to improve the behaviour of the fluid and therefore the results of the core displacement. Different components were suggested to be acquired and implemented as to achieve a better functioning of the setup. The parts designed and the elements proposed had in consideration the difficulties found in the first experiments of the project but also the problems encountered during the recent experiments for the evaluation of the pressure setup.

The study of the structural integrity of the pieces designed was done, confirming the choice of the piece. A study of the fluid dynamics when intersected with certain parts of the setup was addressed to have a better understanding of the internal path of the fluid. The simulations' results suggest that the honeycomb does not significantly impact the velocity of the fluid. Furthermore, it was observed that the force applied by the fluid on the core is of significant magnitude, this is especially highlighted in the unsteady flow simulations, which is expected since a multiphase model is present.

The magnitude of the force obtain through numerical modelling is high enough to confer vertical movement to the core, experiments should be conducted using the designed core attachment pieces to measure the vertical movement of the core. Additionally, new measurements methods should be implemented to validate the obtained results of the Force.

BIBLIOGRAPHY

Croci. 2019. ‘Développement d ’ Un Essai de Validation Pour Un Modèle de Simulation Numérique d ’ Interaction Fluide Structure’. (Internal Project Document)

Croci. 2020. ‘Développement d’un Essai de Validation Pour Un Modèle de Simulation Numérique d’interaction Fluide Structure’. (Internal Project Document)

Loehrke, R. I., and H. M. Nagib. 1976. ‘Control of Free Stream Turbulence By Means of Honeycombs: A Balance Between Suppression and Generation.’ *American Society of Mechanical Engineers (Paper)*, no. 76-FE-2.

Palut, Sous-lieutenant Aymeric. 2021. ‘Etude Du Déport Noyau’.

Sanitas, A., M. Bedel, and M. El Mansori. 2018. ‘Experimental and Numerical Study of Section Restriction Effects on Filling Behavior in Low-Pressure Aluminum Casting’. *Journal of Materials Processing Technology* 254 (April): 124–34. https://doi.org/10.1016/J.JMATPROTEC.2017.11.013.

‘Schlieren Flow Visualization’. n.d. Accessed 16 May 2022. https://www.grc.nasa.gov/www/k-12/airplane/tunvschlrn.html.

‘The Engineering ToolBox’. n.d. Accessed 5 July 2022. https://www.engineeringtoolbox.com/.

‘What Value of Turbulence Intensity Should Be Applied? | CFD | Autodesk Knowledge Network’. n.d. Accessed 22 June 2022. https://knowledge.autodesk.com/support/cfd/learn-explore/caas/sfdcarticles/sfdcarticles/What-value-of-turbulence-intensity-should-be-applied.html.

ANNEX A

Product Specifications

Flow Ranges and Pressure Ratings:

Pressure Controller Model	Pressure Controller Model	Flow Ranges N2 Eq. Ratings		Minimum Full Scale Pressure	Maximum Full Scale Pressure	Pressure Equipment Directive (PED) Module H Category
		Min. F.S.	Max. F.S.	Standard	Standard	
SLA5810/SLAMf10	Downstream (Pressure Regulator)	0.003 0.1	50* 10	1 psi 1500 psi	1500 psia/103 bara 4500 psia/310 bara	Sound Engineering Practices (SEP)
SLA5820/SLAMf20	Upstream (Back Pressure Regulator)	0.003 0.1	50* 10	1 psi 1500 psi	1500 psia/103 bara 4500 psia/310 bara	Sound Engineering Practices (SEP)
SLA5840	Remote Transducer Upstream or Downstream	0.003 0.1	50 10	10 psi 1500 psi	1500 psia/103 bara 4500 psia/310 bara	Sound Engineering Practices (SEP)

* Please see sizing tool for flow limitations < 10 psi F.S. pressure

	SLA58510/20 & SLAMf10/20	SLA5840
PERFORMANCE		
Pressure Accuracy (Including Linearity and Hysteresis)	±0.25% of Transducer F.S., F.S. > 300 psia ±0.12% of Transducer F.S., F.S. ≤ 300 psia	Dependent on Remote Pressure Transducer
Flow Accuracy (N2 equivalent)	N/A	±0.9% of S.P. (20-100% F.S.) ±0.18% of F.S. (2-20% F.S., 1-20% F.S. from 1-50 lpm)
Control Range	20:1 Typical - Application specific	
Repeatability & Reproducibility	0.20% S.P.	
Linearity	Included in accuracy	
Response Time (Settling time within ±2% F.S. for 0-100% command step)	System dependent	<1 second
Zero Stability	< ± 0.001% F.S. per 30 days	Dependent on Remote Pressure Transducer
Temperature Coefficient	±0.1% of F.S. per °C	Dependent on Remote Pressure Transducer
Pressure Coefficient (Flow Measurement Only)	N/A	±0.03% per psi (0-200 psi N2)
Attitude Sensitivity	The accuracy of the Pressure Sensor is not attitude dependent	
RATINGS		
Operating Temperature Range	-14 to 65°C (7 to 149°F)**	
Transducer Pressure Ratings	15 psia/1.03 bara for < 15 psia full scale 15 psig/1.03 barg for < 15 psig full scale 100 psia/6.9 bara for < 100 psia full scale 100 psig/6.9 barg for 15-100 psig full scale 300 psia/20.7 bara for 100-300 psia full scale 300 psig/20.7 barg for 100-300 psig full scale 3000 psia/206.9 bara for 300-3000 psia full scale 4500 psia/310.3 bara for 3000-4500 psia full scale	Dependent on Remote Pressure Transducer
Leak Integrity (external)	$1x10^{-9}$ atm. cc/sec He	
MECHANICAL		
Valve Type	Normally Closed, Normally Open	
Primary Wetted Materials	316L Stainless Steel, High Alloy Stainless Steel, Viton® fluoroelastomers. Optional Buna-N, Kalrez®, Teflon®/Kalrez®, and EPDM	
DIAGNOSTICS		
Status Lights	MFC Health, Network Status	
Alarms*	Sensor Output, Control Valve Output, Over Temperature, Power Surge/Sag, Network Interruption	
Diagnostic/Service Port	RS485 via 2.5 mm jack (Located under the top cover in SLAMf version)	

*Alarm modes are dependent on the communications interface. These are described in the corresponding digital communication interface manual.
**Hazardous area certifications have a temperature range limitation of 0-65°C.

Product Dimensions

SLA5810/20, Thru-Flow, RS485

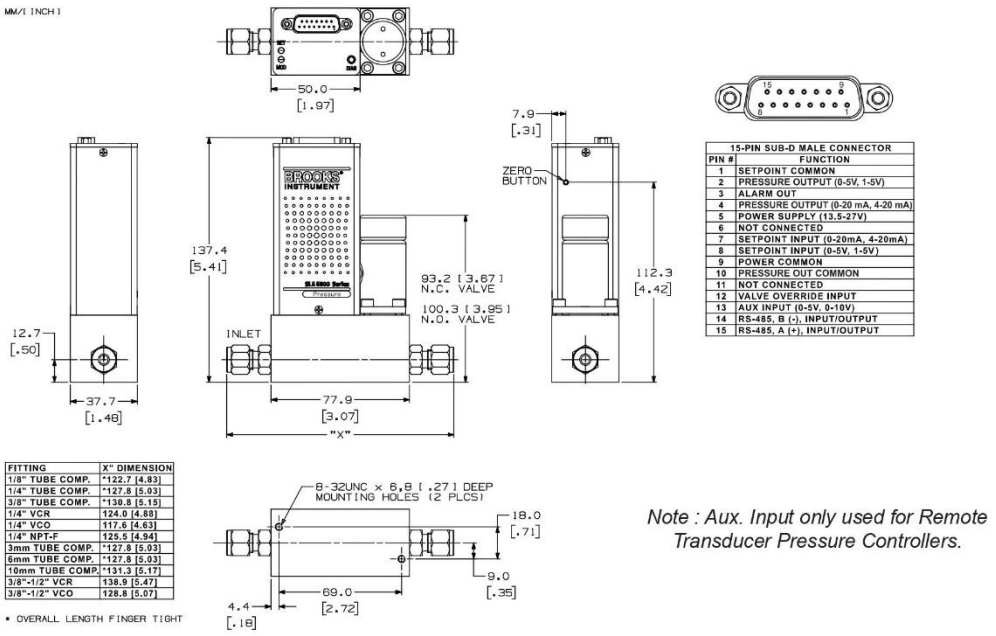

15-PIN SUB-D MALE CONNECTOR	
PIN #	FUNCTION
1	SETPOINT COMMON
2	PRESSURE OUTPUT (0-5V, 1-5V)
3	ALARM OUT
4	PRESSURE OUTPUT (0-20 mA, 4-20 mA)
5	POWER SUPPLY (13.5-27V)
6	NOT CONNECTED
7	SETPOINT INPUT (0-20mA, 4-20mA)
8	SETPOINT INPUT (0-5V, 1-5V)
9	POWER COMMON
10	PRESSURE OUT COMMON
11	NOT CONNECTED
12	VALVE OVERRIDE INPUT
13	AUX INPUT (0-5V, 0-10V)
14	RS-485, B (-), INPUT/OUTPUT
15	RS-485, A (+), INPUT/OUTPUT

FITTING	X" DIMENSION
1/8" TUBE COMP.	*122.7 [4.83]
1/4" TUBE COMP.	*127.8 [5.03]
3/8" TUBE COMP.	*130.8 [5.15]
1/4" VCR	124.0 [4.88]
1/4" VCO	117.6 [4.63]
1/4" NPT-F	125.5 [4.94]
3mm TUBE COMP.	*127.8 [5.03]
6mm TUBE COMP.	*127.8 [5.03]
10mm TUBE COMP.	*131.3 [5.17]
3/8"-1/2" VCR	138.9 [5.47]
3/8"-1/2" VCO	128.8 [5.07]

* OVERALL LENGTH FINGER TIGHT

Note : Aux. Input only used for Remote Transducer Pressure Controllers.

SLA5810/20, Thru-Flow, Profibus

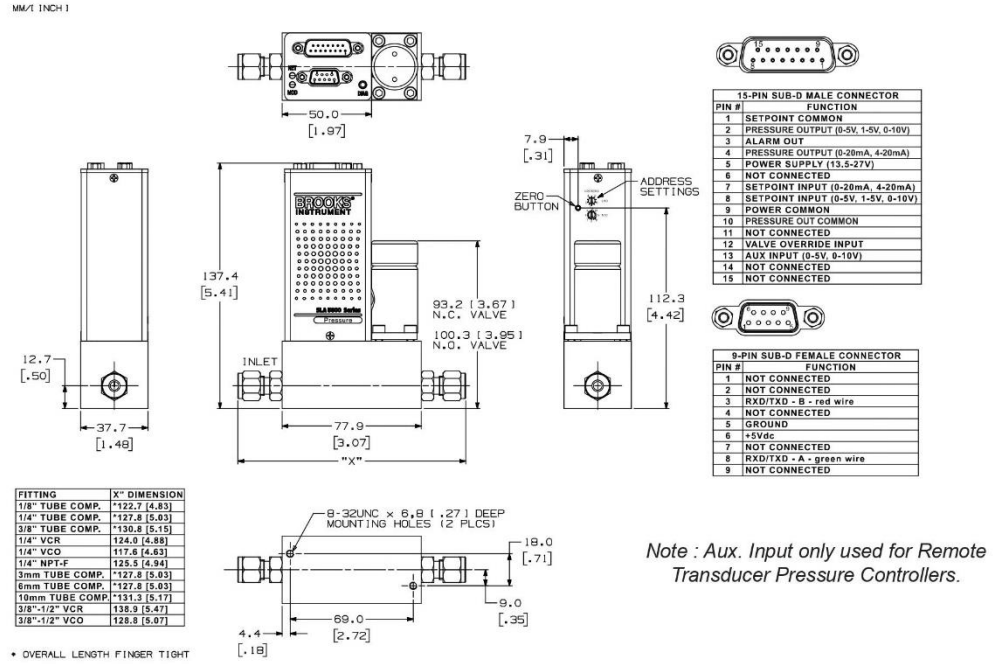

15-PIN SUB-D MALE CONNECTOR	
PIN #	FUNCTION
1	SETPOINT COMMON
2	PRESSURE OUTPUT (0-5V, 1-5V, 0-10V)
3	ALARM OUT
4	PRESSURE OUTPUT (0-20mA, 4-20mA)
5	POWER SUPPLY (13.5-27V)
6	NOT CONNECTED
7	SETPOINT INPUT (0-20mA, 4-20mA)
8	SETPOINT INPUT (0-5V, 1-5V, 0-10V)
9	POWER COMMON
10	PRESSURE OUT COMMON
11	NOT CONNECTED
12	VALVE OVERRIDE INPUT
13	AUX INPUT (0-5V, 0-10V)
14	NOT CONNECTED
15	NOT CONNECTED

9-PIN SUB-D FEMALE CONNECTOR	
PIN #	FUNCTION
1	NOT CONNECTED
2	NOT CONNECTED
3	RXD/TXD - B - red wire
4	NOT CONNECTED
5	GROUND
6	+5Vdc
7	NOT CONNECTED
8	RXD/TXD - A - green wire
9	NOT CONNECTED

FITTING	X" DIMENSION
1/8" TUBE COMP.	*122.7 [4.83]
1/4" TUBE COMP.	*127.8 [5.03]
3/8" TUBE COMP.	*130.8 [5.15]
1/4" VCR	124.0 [4.88]
1/4" VCO	117.6 [4.63]
1/4" NPT-F	125.5 [4.94]
3mm TUBE COMP.	*127.8 [5.03]
6mm TUBE COMP.	*127.8 [5.03]
10mm TUBE COMP.	*131.3 [5.17]
3/8"-1/2" VCR	138.9 [5.47]
3/8"-1/2" VCO	128.8 [5.07]

* OVERALL LENGTH FINGER TIGHT

Note : Aux. Input only used for Remote Transducer Pressure Controllers.

ANNEX B

MINI SPOOL VALVES
solenoid air operated
Ø M5 - G1/8 - G1/4 tapped body
adaptable on joinable subbases

5/2-5/3
Series
519-520-521

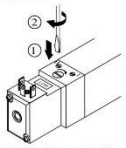

GENERAL

Fluid		Air or neutral gaz, filtered, lubricated or not
Operating pressure		1,5 to 8 bar
Ambient temperature		+5°C to +50°C
Orifice size		519 : 2,5 mm; 520 : 4 mm; 521 : 6 mm
Flow (Qv at 6 bar)	series 519	175 l/min (ANR) - Kv : 2,5
	series 520	600 l/min (ANR) - Kv : 8,5
	series 521	1050 l/min (ANR) - Kv : 15

CONSTRUCTION

SPOOL VALVES	
Body	Anodised white aluminium
Cover	POM (polyacetal)
Internal parts	Stainless steel, light alloy and POM (polyacetal)
Seals	NBR (nitrile)
Manual operator	Maintained, impulse Latchable in hold position (push-turn)
PILOT	
Seals	NBR (nitrile)
Electrical equipment	Conforming to NF C79300 standard
Coil and iron circuit	Encapsulated

ELECTRICAL CHARACTERISTICS

	voltages	consumption	insulation class	protection degree	electrical connection
~	24V, 115V, 230V - 50/60Hz	2 VA (1,5 W)	F	IP 65	spade plug size 15 connector, DIN 43650, 9,4 mm, industry standard B, rotatable by 90°
=	24V	1,6 W			

SPECIFICATIONS

function symbol		operators: solenoid air operated, pilot (14), return (12)	response time (ms) energized	response time (ms) de-energized	voltages	catalogue number serie 519	serie 520	serie 521
5/2		spring return	20	30	24V ~	-	52000386	-
					115V ~	-	52000387	-
					230V ~	-	52000388	-
					24V =	-	52000380	52100401
		differential return	20	30	24V ~	51900002	52000002	52100002
					115V ~	51900003	52000003	52100003
					230V ~	51900004	52000004	52100004
					24V =	51900001	52000001	52100001
	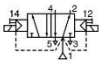	solenoid air return	20	-	24V ~	51900006	52000006	52100006
					115V ~	51900007	52000007	52100007
					230V ~	51900008	52000008	52100008
					24V =	51900005	52000005	52100005
5/3	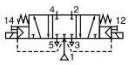	pressure held **W1**	20	50	24V ~	51900010	52000010	52100010
					115V ~	51900011	52000011	52100011
					230V ~	51900012	52000012	52100012
					24V =	51900009	52000009	52100009
	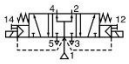	pressure applied **W2**	20	50	24V ~	51900126	52000126	52100126
					115V ~	51900127	52000127	52100127
					230V ~	51900128	52000128	52100128
					24V =	51900129	52000129	52100129
	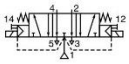	pressure release **W3**	20	50	24V ~	51900087	52000087	52100087
					115V ~	51900088	52000088	52100088
					230V ~	51900089	52000089	52100089
					24V =	51900090	52000090	52100090

OPTIONS AND ACCESSORIES

UR approval « UL Recognized »		24V =/~	612102
visual indicator (LED) and electrical protection ( )		24V =/~	88130401
		115V ~	88130402
		230V ~	88130403
connector size 15 with cable, 2 m long			88143567
connector size 15 with built-in visual indication and protection, with cable outlet, 2 m long	( )	24V =/~	88143580
flange for ports 2 - 4 with instant fittings for flexible tube 6 mm O.D. (series 520)			88135532

SUBBASES : possible mounting on joinable subbases ( ). Fixing screws and seals are supplied with subbases

All leaflets are available on: **www.asco.com**

34 - Pneumatic Valves (5/2 - 5/3)

DIMENSIONS (mm), WEIGHT (kg)

5/2 differential return and spring return

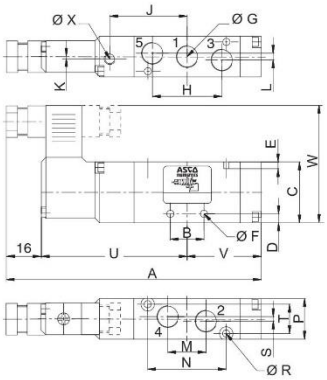

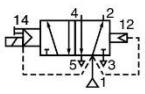

series	A	V
519	97,5	25
520	114	33,2
521	131,3	41,6

weight	
519	0,085
520	0,095
521	0,155

	series	B	C	D	E	ØF	ØG	H	J	K	L	M	N	P	ØR	S	T	U	W	ØX
5/2	519	11	26	4	4	3,3	M5	21,6	26	-	-	11	19	15	2,7	6	11	56,5	52	4
	520	15	27	6	3	3,3	G1/8	32,4	34,3	1	3	16,2	35	18	3,2	-	13	64,8	54,5	4
	521	22	31	6,5	4	4,3	G1/4	44	43,2	-	4	22	50	22	4,2	4	16	73,7	56,5	3

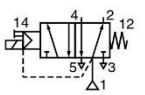

series	A	V
519	97,5	-
520	123,3	42,5
521	131,3	-

5/2 solenoid air return

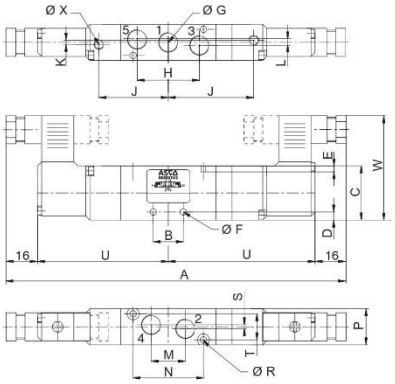

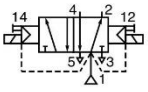

weight	
519	0,135
520	0,160
521	0,200

	series	A	B	C	D	E	ØF	ØG	H	J	K	L	M	N	P	ØR	S	T	U	W	ØX
5/2	519	145	11	26	4	4	3,3	M5	21,6	26	-	-	11	19	15	2,7	6	11	56,5	52	4
	520	161,5	15	27	6	3	3,3	G1/8	32,4	34,3	2	3	16,2	35	18	3,2	-	13	64,8	54,5	4
	521	179,5	22	31	6,5	4	4,3	G1/4	44	43,2	-	4	22	50	22	4,2	4	16	73,7	56,5	3

5/3 solenoid air return

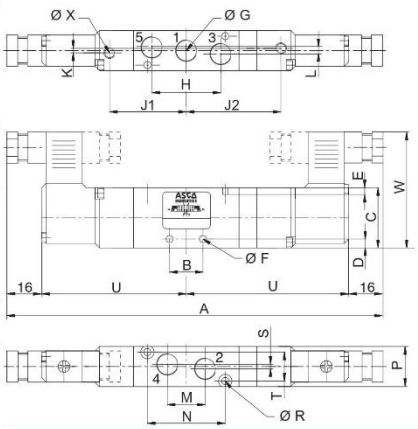

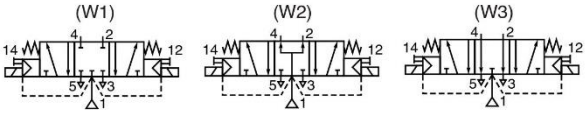

	series	A	B	C	D	E	ØF	ØG	H	J1	J2	K	L	M	N	P	ØR
5/3	519	153	11	26	4	4	3,3	M5	21,6	26	34	-	-	11	19	15	2,7
	520	170,3	15	27	6	3	3,3	G1/8	32,4	34,3	43,3	1	3	16,2	35	18	3,2
	521	188,3	22	31	6,5	4	4,3	G1/4	44	43,2	52,1	-	4	22	50	22	4,2

	series	S	T	U	V	W	ØX	weight
5/3	519	6	11	56,5	64,5	52	4	0,140
	520	-	13	64,8	73,7	54,5	4	0,170
	521	4	16	73,7	82,6	56,5	3	0,210

APPENDIX A

The simulations performed in the Chapter 5 had the same Default controls, except for the multiphase unsteady simulations where a volumetric control need to be implemented, where the number of prism layers in a part of the subtract was changed. For the generation of the mesh several Default Controls were altered:

- the Base Size had a value of 1 mm;
- the Number of Prism Layers was 8;
- the Prism Layer Total Thickness had a size type absolute, a percentage base of 200 and an absolute size of 2 mm;
- the Minimum Surface Size has a size type of relative to base, a percentage of base of 50 and an absolute size of 5×10^{-4} m;
- the Maximum Tet Size had a size type of relative to base, a percentage of base of 10000 and an absolute size of 0.1m.

In the Figure A.1 and Figure A.2 is possible to see the generated mesh for the steady and multiphase unsteady simulations in the honeycomb. This component, due to its complex geometry for the generation of the mesh, was used as reference for the alteration of the parameters of the Default Control for the achievement of a more refined mesh in the Subtract.

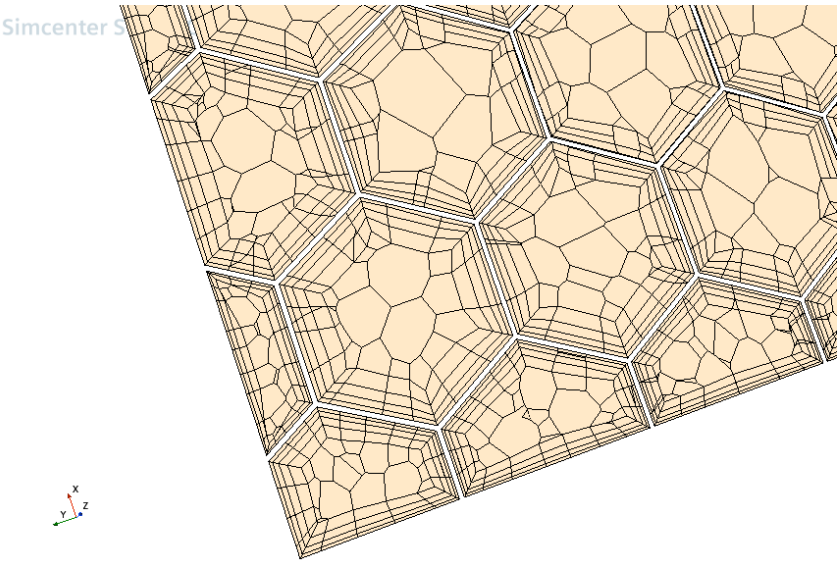

Figure A.1. Mesh in the honeycomb for steady simulations.

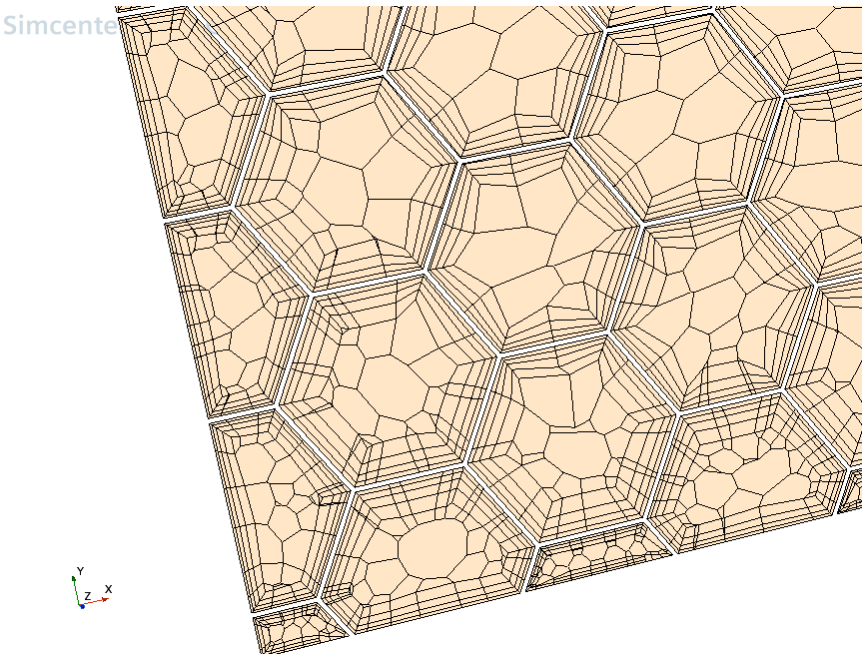

Figure A.2. Mesh in the honeycomb for multiphase unsteady simulations.

APPENDIX B

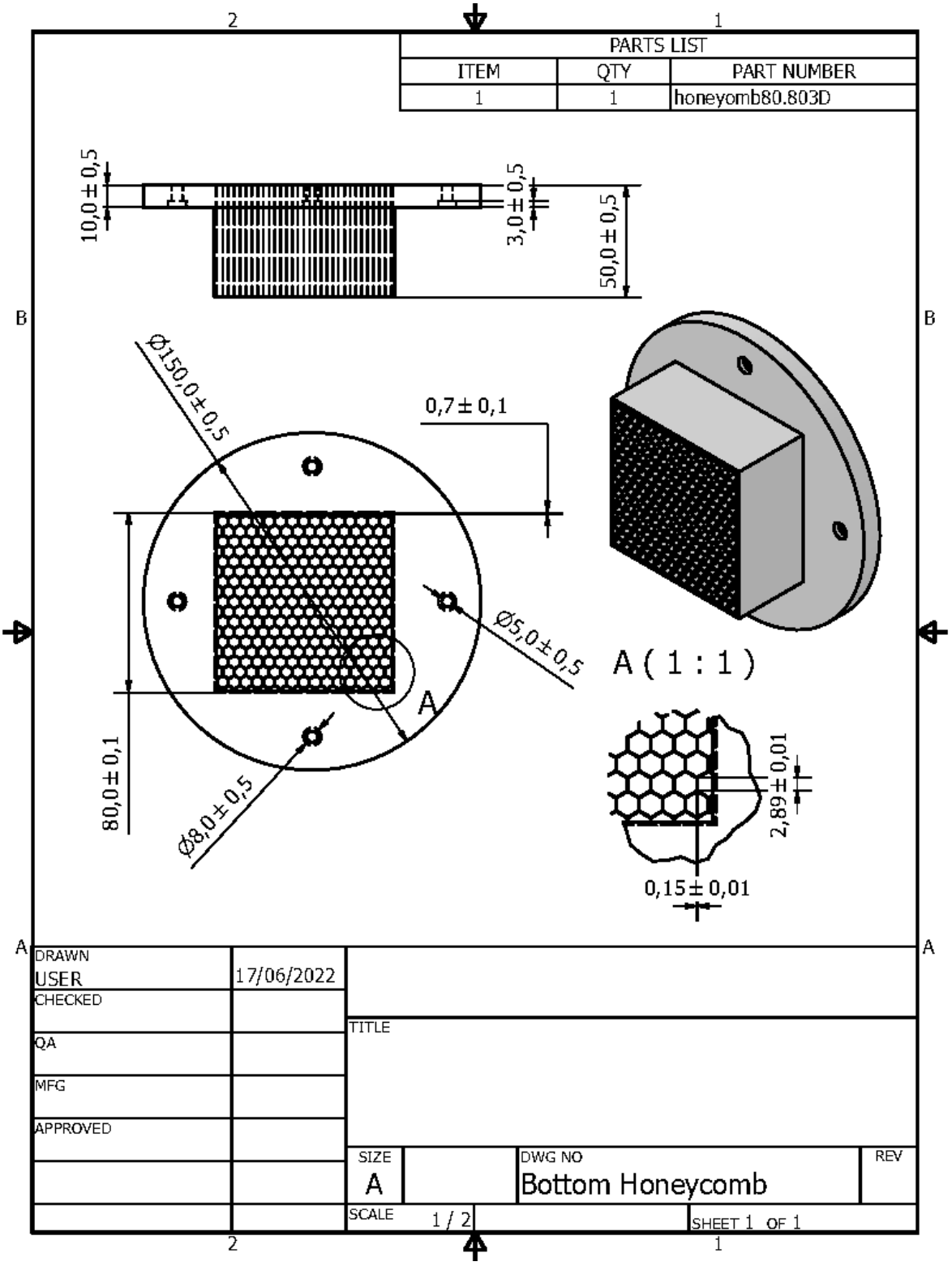
PARTS LIST
ITEM | QTY | PART NUMBER
1 | 1 | honeyomb80.803D
10,0 ± 0,5
3,0 ± 0,5
50,0 ± 0,5
Ø150,0±0,5
0,7 ± 0,1
Ø5,0±0,5
A
80,0 ± 0,1
Ø8,0±0,5
A (1 : 1)
2,89 ± 0,01
0,15 ± 0,01
DRAWN
USER
17/06/2022
CHECKED
QA
MFG
APPROVED
TITLE
SIZE
A
DWG NO
Bottom Honeycomb
REV
SCALE
1 / 2
SHEET 1 OF 1

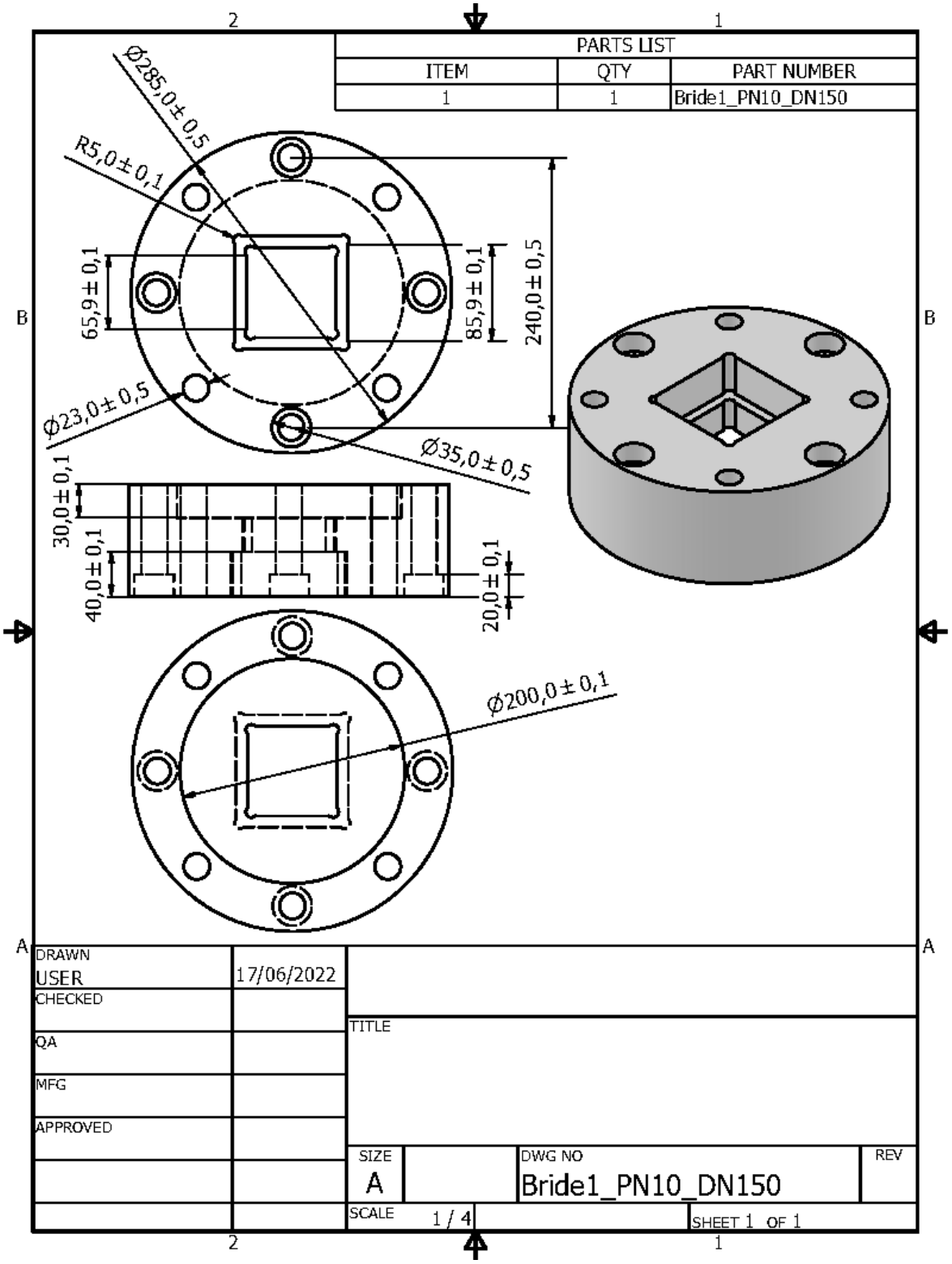
PARTS LIST
ITEM
QTY
PART NUMBER
1
1
Bride1_PN10_DN150
Ø285,0±0,5
R5,0±0,1
65,9±0,1
85,9±0,1
240,0±0,5
Ø23,0±0,5
Ø35,0±0,5
30,0±0,1
40,0±0,1
20,0±0,1
Ø200,0±0,1
DRAWN
USER
17/06/2022
CHECKED
QA
MFG
APPROVED
TITLE
SIZE
A
DWG NO
Bride1_PN10_DN150
REV
SCALE
1 / 4
SHEET 1 OF 1

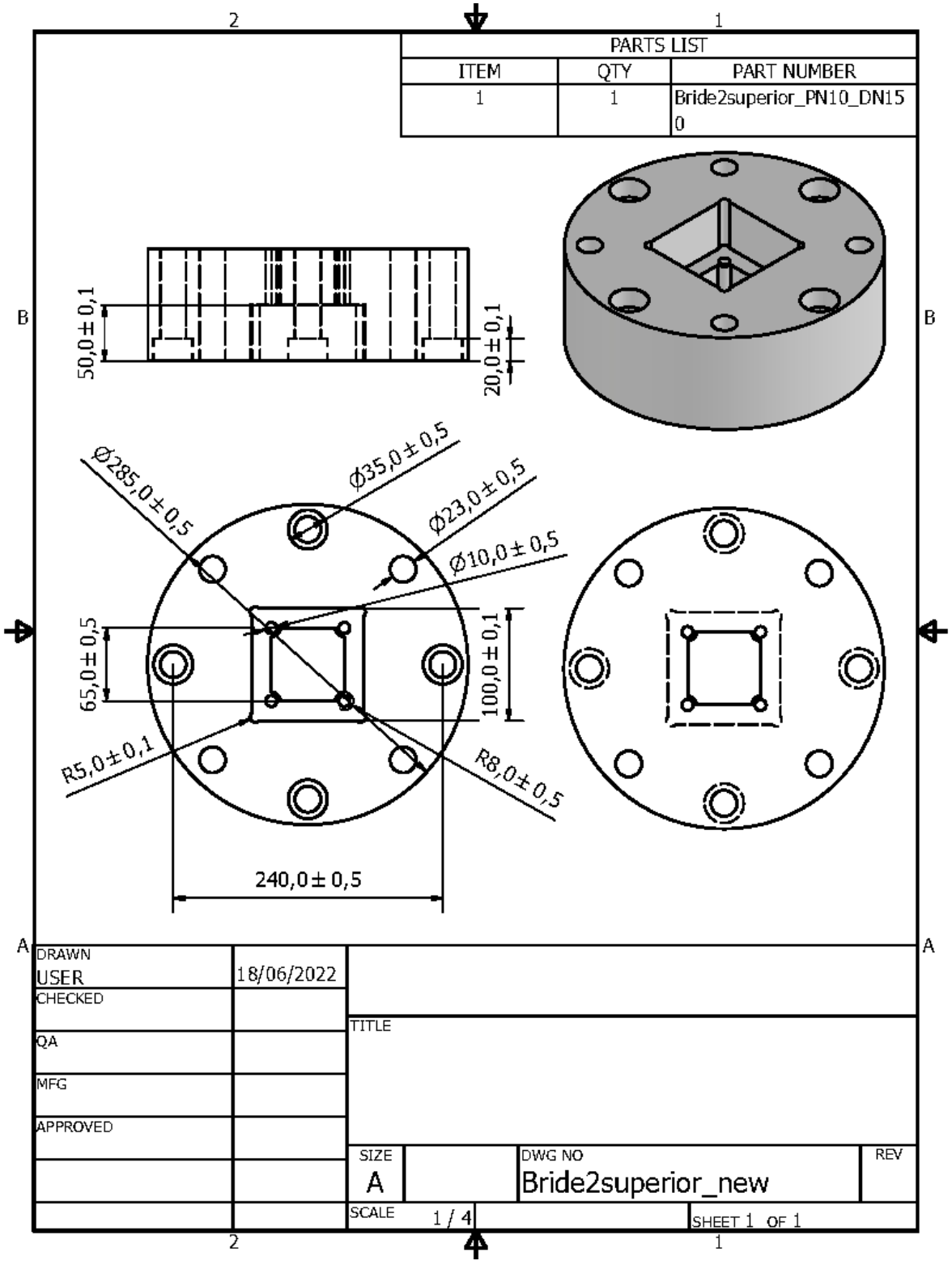
PARTS LIST
ITEM
QTY
PART NUMBER
1
1
Bride2superior_PN10_DN150
50,0 ± 0,1
20,0 ± 0,1
Ø285,0 ± 0,5
Ø35,0 ± 0,5
Ø23,0 ± 0,5
Ø10,0 ± 0,5
65,0 ± 0,5
100,0 ± 0,1
R5,0 ± 0,1
R8,0 ± 0,5
240,0 ± 0,5
DRAWN
USER
18/06/2022
CHECKED
QA
MFG
APPROVED
TITLE
SIZE
A
DWG NO
Bride2superior_new
REV
SCALE
1 / 4
SHEET 1 OF 1

PARTS LIST		
ITEM	QTY	PART NUMBER
1	1	Square piece

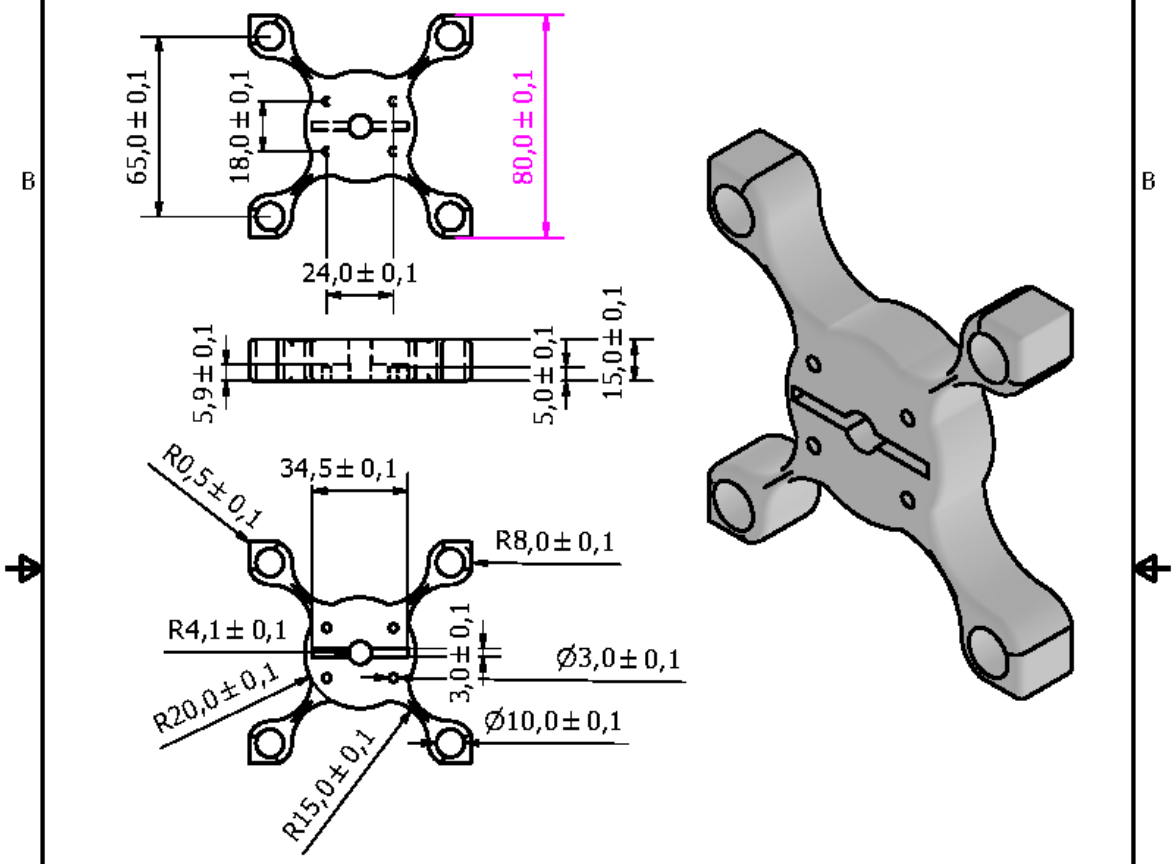

DRAWN USER	18/06/2022		
CHECKED		TITLE	
QA			
MFG			
APPROVED		SIZE A	DWG NO Ceramic Core Attchment Piece REV
		SCALE 1 : 1	SHEET 1 OF 1

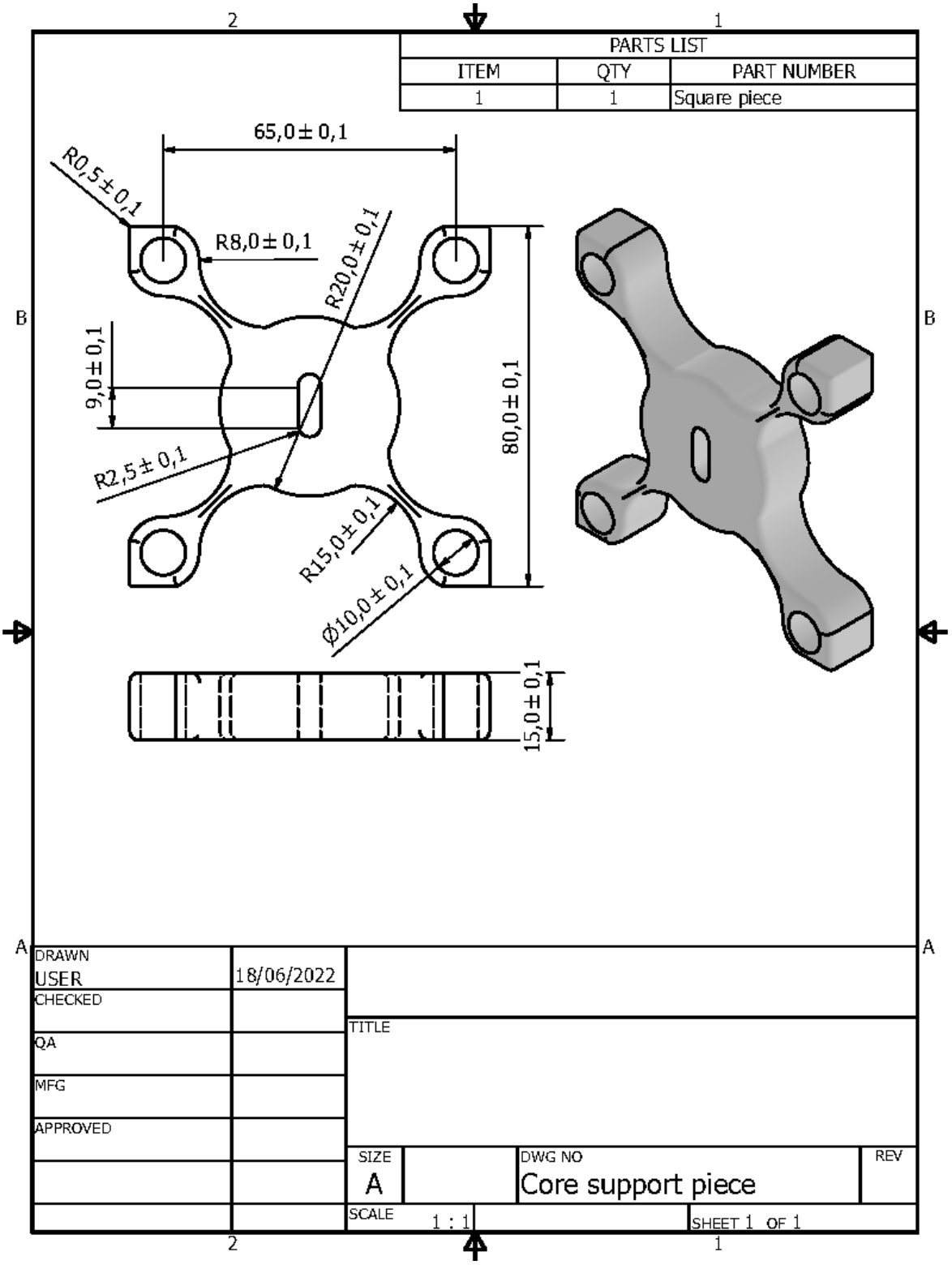
PARTS LIST
ITEM
QTY
PART NUMBER
1
1
Square piece
65,0 ± 0,1
R0,5 ± 0,1
R8,0 ± 0,1
R20,0 ± 0,1
9,0 ± 0,1
80,0 ± 0,1
R2,5 ± 0,1
R15,0 ± 0,1
Ø10,0 ± 0,1
15,0 ± 0,1
DRAWN
USER
18/06/2022
CHECKED
QA
MFG
APPROVED
TITLE
SIZE
A
DWG NO
Core support piece
REV
SCALE
1 : 1
SHEET 1 OF 1

PARTS LIST		
ITEM	QTY	PART NUMBER
1	1	honeyomb80.803D

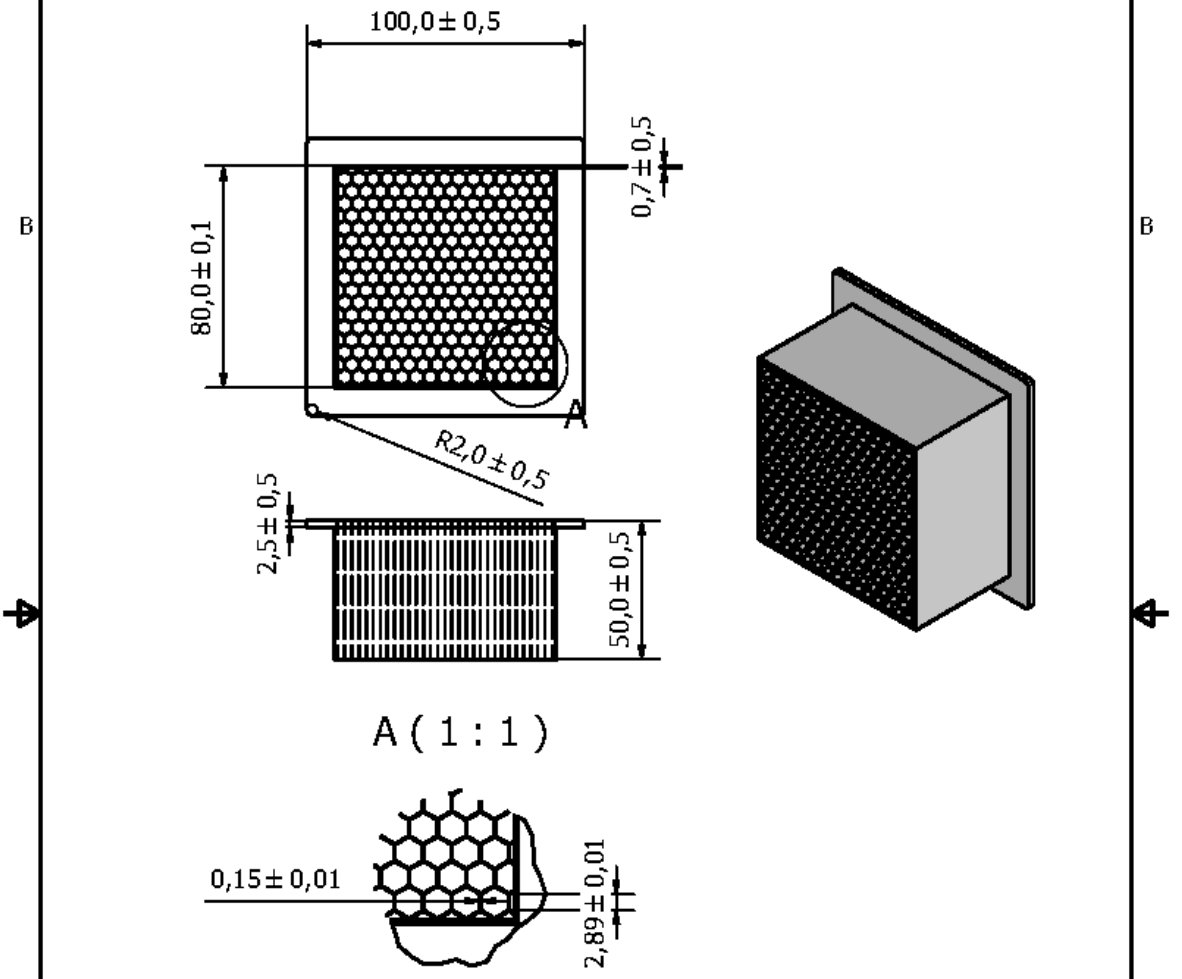

DRAWN USER	18/06/2022			
CHECKED		TITLE		
QA				
MFG				
APPROVED		SIZE A	DWG NO Honeycomb	REV
		SCALE 1 / 2		SHEET 1 OF 1

PARTS LIST		
ITEM	QTY	PART NUMBER
1	1	inside part

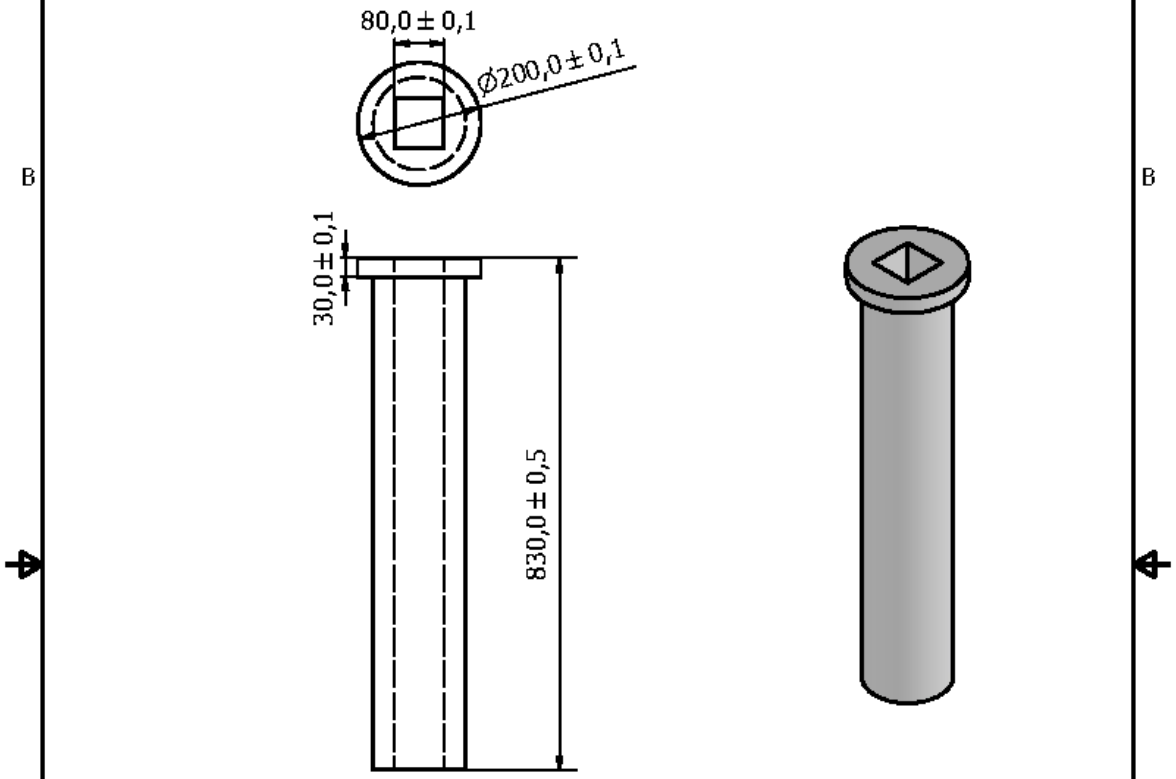

DRAWN USER	17/06/2022			
CHECKED		TITLE		
QA				
MFG				
APPROVED		SIZE A	DWG NO Internal Piece	REV
		SCALE 0.11 : 1	SHEET 1 OF 1	

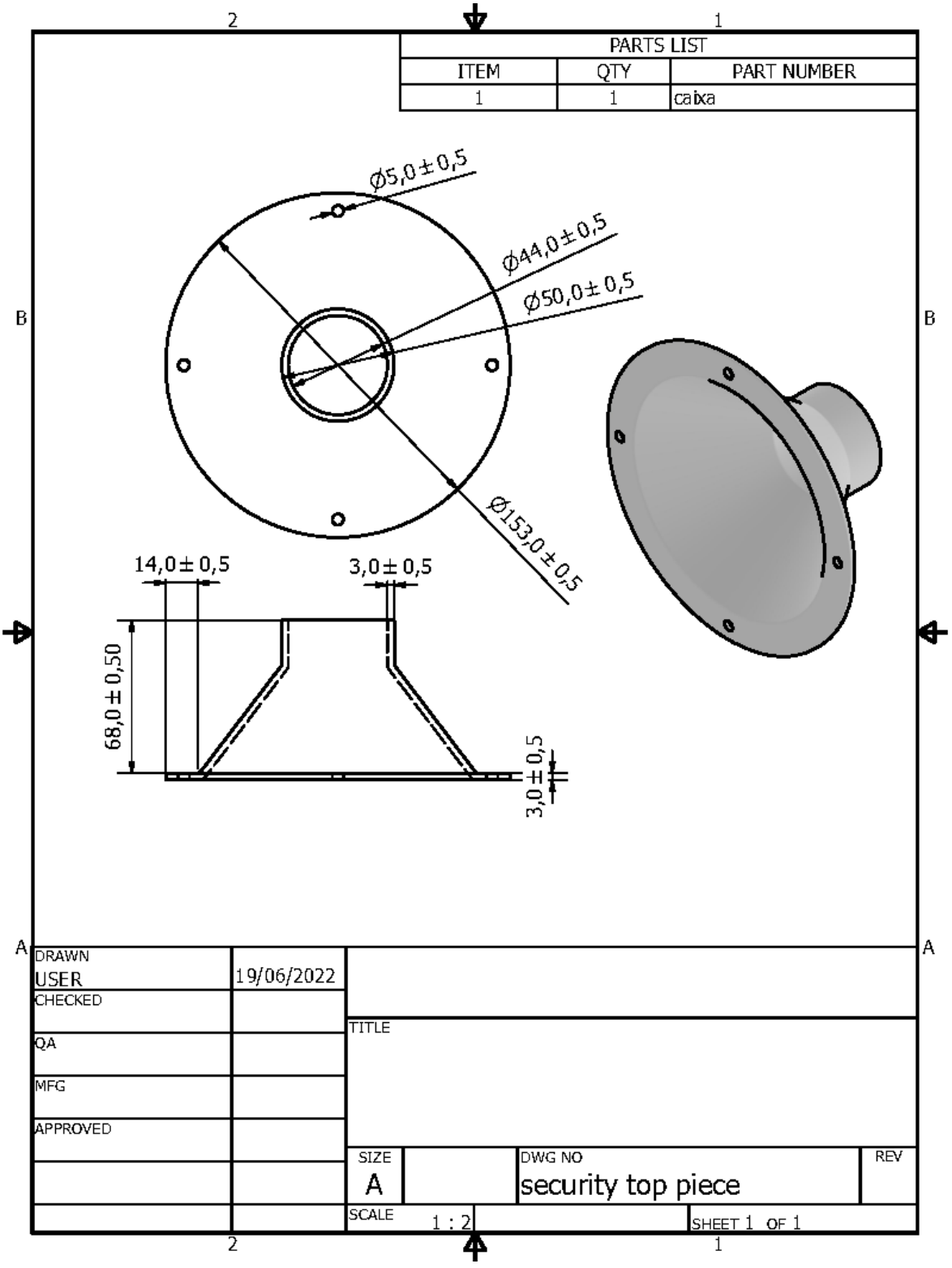
PARTS LIST
ITEM
QTY
PART NUMBER
1
1
caixa
Ø5,0±0,5
Ø44,0±0,5
Ø50,0±0,5
Ø153,0±0,5
14,0±0,5
3,0±0,5
68,0±0,50
3,0±0,5
DRAWN
USER
19/06/2022
CHECKED
QA
MFG
APPROVED
TITLE
SIZE
A
DWG NO
security top piece
REV
SCALE
1 : 2
SHEET 1 OF 1

PARTS LIST		
ITEM	QTY	PART NUMBER
1	4	1 veine part

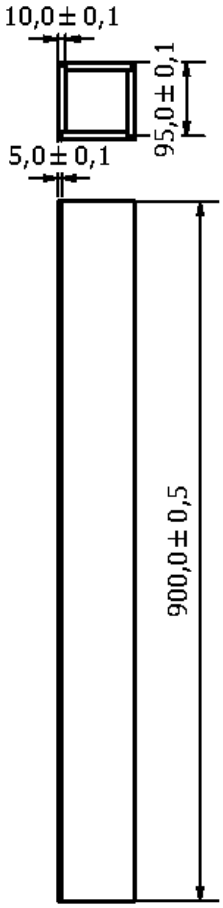

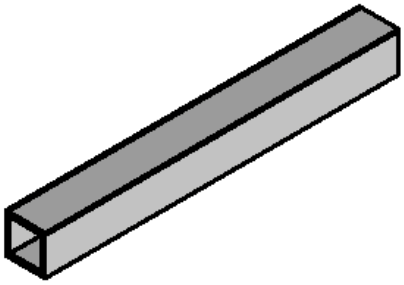

DRAWN	USER	18/06/2022		
CHECKED			TITLE	
QA				
MFG				
APPROVED				
			SIZE: A	DWG NO: Vein
			SCALE: 1 / 10	SHEET 1 OF 1